The 26 November 2019 Durrës earthquake, Albania: coseismic displacements and occurrence of slow slip events in the year following the earthquake

Kristina Matraku, François Jouanne, Edmond Dushi, Rexhep Koçi, Neki Kuka, Raphael Grandin, Pascale Bascou

Geophysical Journal International

Geophys. J. Int. (2023) **234,** 807–838
Advance Access publication 2023 March 14
GJI Geodynamics and tectonics

https://doi.org/10.1093/gji/ggad101

The 26 November 2019 Durrës earthquake, Albania: coseismic displacements and occurrence of slow slip events in the year following the earthquake

Kristina Matraku [1,2] François Jouanne,[1] Edmond Dushi [2] Rexhep Koçi,[2] Neki Kuka,[2] Raphael Grandin [3] and Pascale Bascou [1]

[1] *Université Grenoble Alpes, Université Savoie Mont Blanc, CNRS, ISTerre, Université Gustave Eiffel,* 38000 *Grenoble, France.*
E-mail: kristina.matraku@univ-smb.fr
[2] *Institute of GeoSciences Energy Water and Environment, Polytechnic University of Tirana, Tiranë* 1000*, Albania.*
[3] *Institut de Physique du Globe de Paris, UMR* 7154*, Sorbonne Paris Cité, Université Paris Diderot,* 75013 *Paris, France*

Accepted 2023 March 6. Received 2023 February 28; in original form 2022 June 30

SUMMARY

Outer Albanides experienced a seismic sequence starting on 21 September 2019, with an M_w 5.6 earthquake, considered a foreshock, and culminated with the main shock on 26 November 2019, followed by a paramount aftershock activity. We propose a model for the coseismic slip distribution using InSAR, permanent, and campaign GNSS measurements. We tested two hypotheses: an earthquake on a thrust plane with the direction N160° and along with a back thrust. By varying the depth and dip angle for the first hypothesis and only the dip angle for the second hypothesis, we concluded the optimal solution is a blind thrust at a 15-km depth dipping eastward 40°, a maximum slip of 1.4 m and an M_w 6.38. A GNSS time-series obtained after 2020 shows two slow slip events (SSEs): the first one is 200 d after the main shock up to 26 d, and the second one is 300 d after the main shock up to 28 d. We tested three hypotheses: SSE along the basement thrust where the main shock has been localized, SSE along the flat formed by the detachment layer of the cover, and SSE along these two faults. We concluded that SSE occurred along the detachment layer or along the two faults.

Key words: Space geodetic surveys; Transient deformation; Europe; Time-series analysis; Continental tectonics: compressional; Fractures, faults and high strain deformation zones; Albania Durrës earthquake; Slow slip events (SSE).

1 INTRODUCTION

1.1 Geological setting

Outer Albanides is a thick-skinned fold-and-thrust belt (Dalipi 1985; Bare *et al.* 1996; Frashëri *et al.* 2009, 1996; Papa & Kondo 1968; Nishani 1985; Valbona & Misha 1987; Dhima *et al.* 1996; Guri & Guri 1996; Mëhillka *et al.* 1996, 1999; Seitaj *et al.* 1996; Velaj 1999; Xhufi & Canaj 1999; Aliaj *et al.* 2010, 2012). It involves a sedimentary series above a detachment level formed by Triassic evaporites (Velaj 2001). The deformed sedimentary series includes a thick post-Serravallian sedimentary series belonging to the peri-Adriatic basin (Frashëri *et al.* 2009). The seismic profile (Fig. 1) shows, in particular, a marked unconformity between molasse formations and the formations of the Ionian and Kruja series, characterized by a series of folds conditioned not by overthrusts but mainly by back thrusts.

The Outer Albanides are structured by NNW–SSE to NW–SE thrusts, back thrusts and folds, and transverse strike-slip faults with a NE–SW to nearly E–W orientation and are characterized by an echelon arrangement of folds, thrusts and back thrusts (Aliaj *et al.* 2012), suggesting a strike-slip component (Biermanns *et al.* 2019). On both sides of the transverse Lezha fault (Fig. 2), the Plio-Quaternary fold axis changes from N125° north to N160° south of the fault. There is also a fold-like change, mainly from the Mesozoic formations to the north and Pliocene to the south. This change suggests the deformed sedimentary pile is much thicker to the south than to the north of the fault. Therefore, the Lezha fault would be a major transfer fault separating two regions subject to different compressive tectonics. These structures are buried under Quaternary marine deposits. The tectonics of Outer Albania show significant pre-Pliocene and post-Pliocene compression, which forms the Periadriatic Depression (Roure *et al.* 2004).

From Durrës to Tirana, the very top section of the cover is also well-evidenced by shallow boreholes sequences and seismic profiles. Based on the analysis of seismic sections, for hydrocarbon exploration, the presence of the thrust and back thrust faults is well-marked in the tectonic environment, affecting post-Messinian and

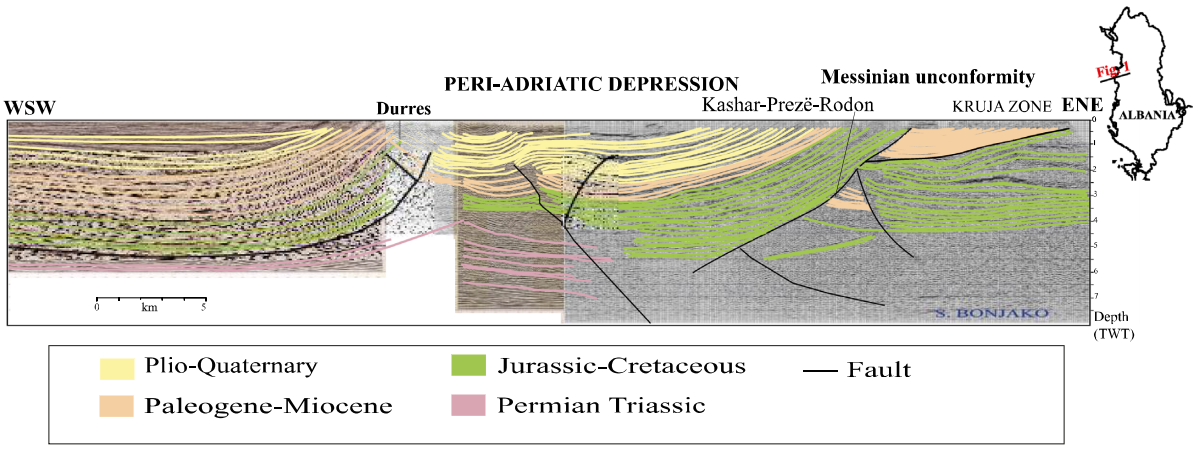

Figure 1. Migrated regional seismic profile, Adriatic Sea-Durrës-Lezha. Fig. 2 shows the location of the profile.

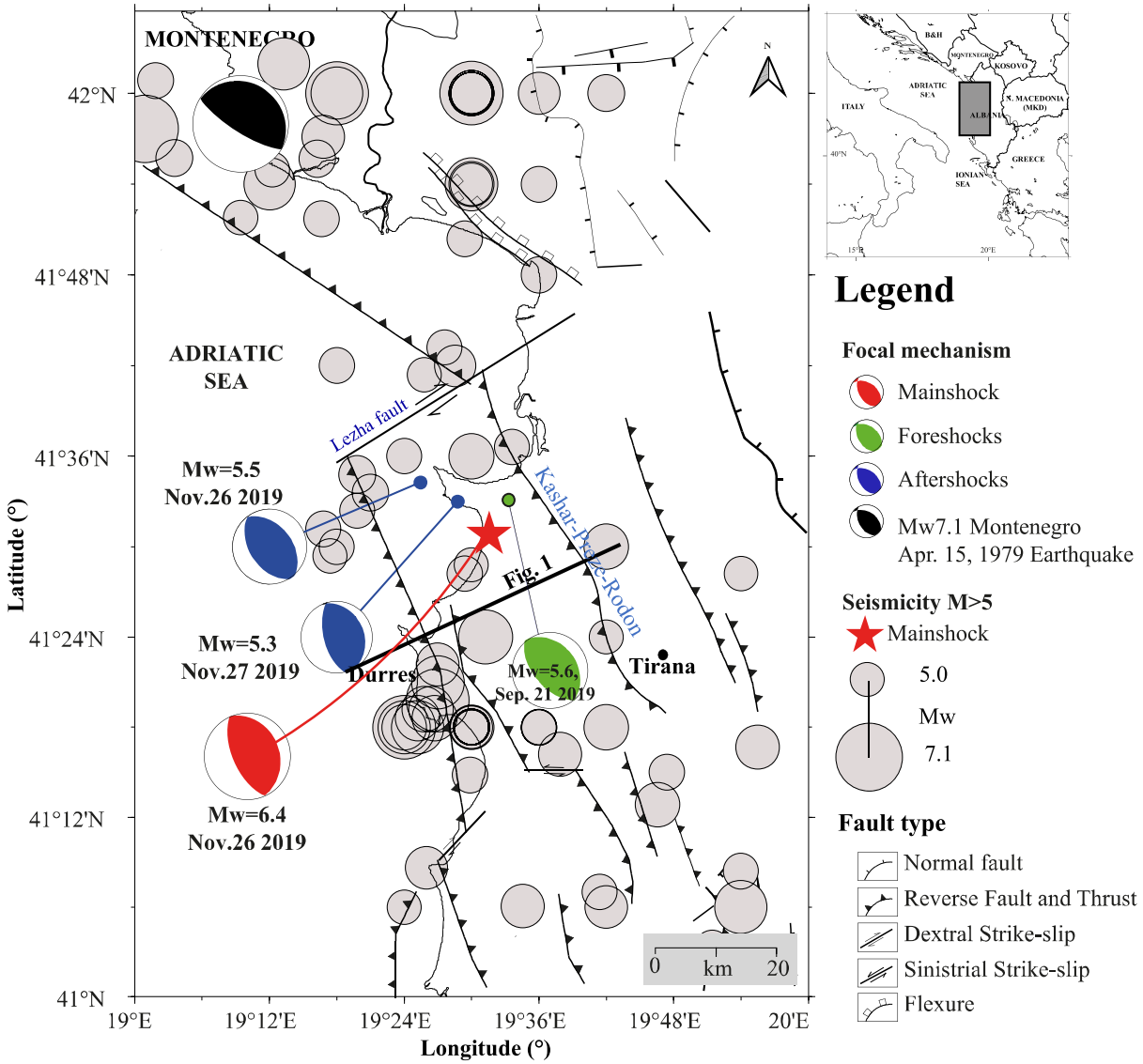

Figure 2. Map of seismic activity ($M_w > 5.0$) around Durrës area, from 58BC till 27 November 2019 (compilation of Sulstarova, E. 1996 and IGEO catalogues). Focal mechanisms are indicated for the main shock (26 November 2019, M_w 6.4), foreshock (21 September 2019, M_w 5.6) and two aftershocks (26 November 2019, M_w 5.5 and 27 November 2019, M_w 5.3; USGS location) and for the Montenegro 15 April 1979, M_w 7.1 event (Benetatos & Kiratzi 2006). The black line represents the location of the seismic profile (see Fig. 1).

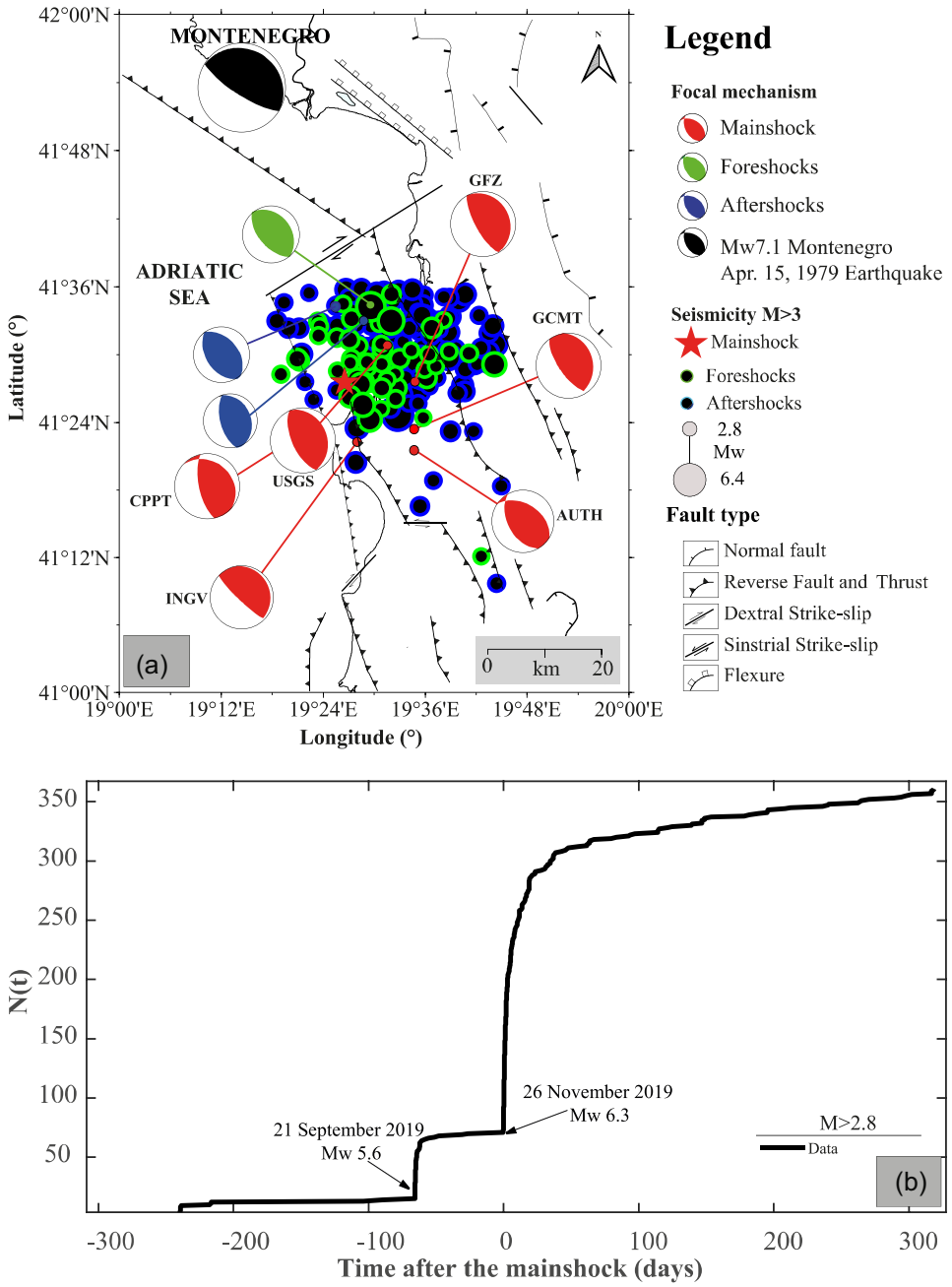

Figure 3. (a) Map of seismic activity in Durrës area, showing foreshocks, the main shock with focal mechanisms from various agencies and aftershocks. Focal mechanisms of 26 November 2019, 02:54 UTC earthquake by different sources (Table 1). Focal mechanisms of the M_w 7.1 Montenegro earthquake 15 April 1979. Source (Benetatos & Kiratzi 2006). Focal mechanisms of M_w 5.6 21 September 2019, foreshock. *Source*: https://earthquake.usgs.gov/earthquakes/eventpage/us60005lrf/moment-tensor) Focal mechanisms of M_w 5.5 26 November 2019, 06:08 UTC aftershocks. *Source*: (https://earthquake.usgs.gov/earthquakes/eventpage/us70006d2z/moment-tensor) Focal mechanisms of M_w 5.3 27 November 2019, 14:45:23 UTC aftershocks. *Source*: (https://earthquake.usgs.gov/earthquakes/eventpage/us70006dsc/moment-tensor). (b) Time decay of the cumulative number of earthquakes (blue line) with magnitude $M_L \geq 2.8$, from 1 March 2019 to 17 November 2020. *Source*: IGEO. The black circles correspond to increased seismic activity. (c) Magnitude versus time for all earthquakes. (d) The cumulative number of events versus magnitude of IGEO catalogue (IGEO catalog 2022) (Gutenberg–Richter law).

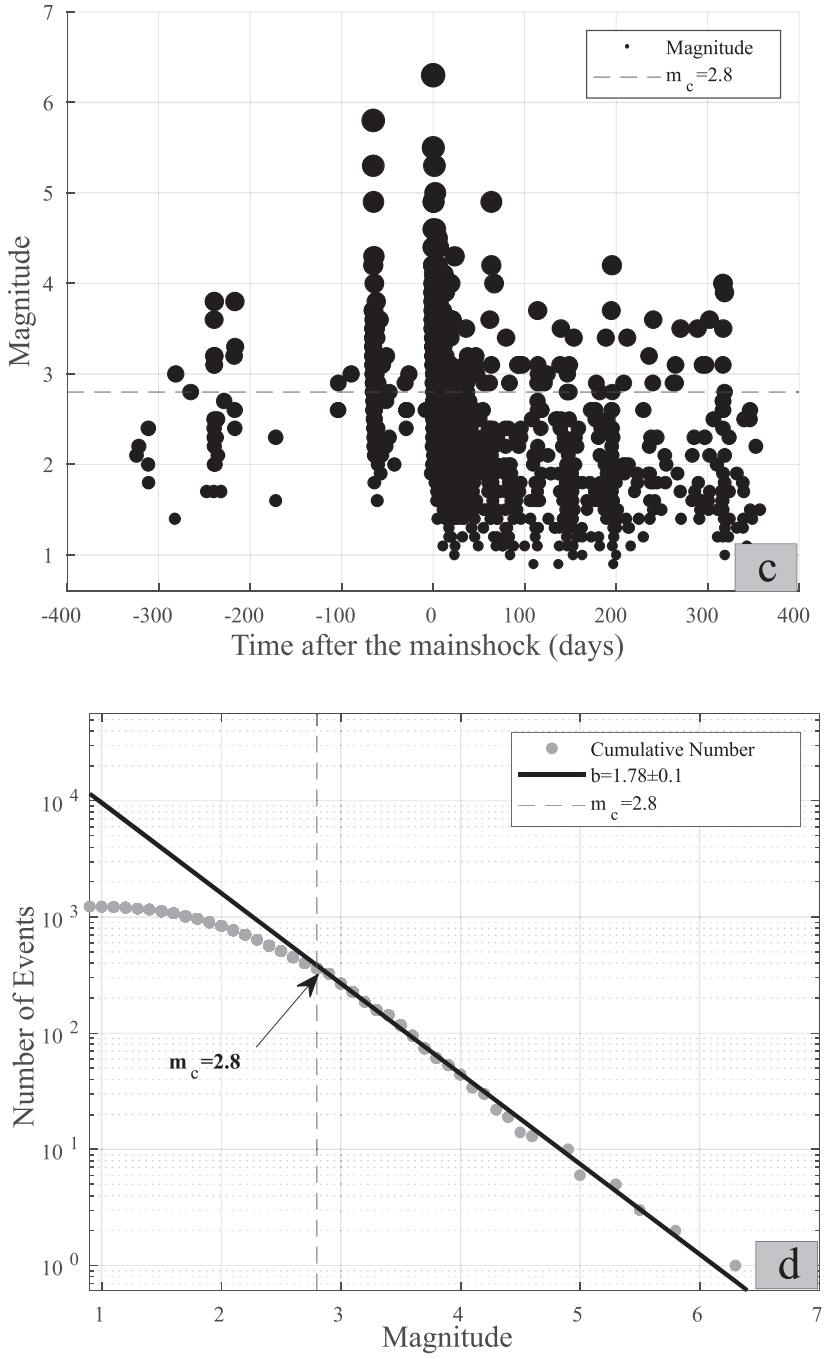

Figure 3. Continued.

Pliocene formations (Fig. 1). The erosional surface is associated with the Messinian formations at the base of the deposits, in contact through the Preza monocline back thrust fault (Fig. 2). Although it is essential to evidence the upper 10 km of the geological structure, these seismic sections do not permit to glance at the basement structure, which is probably deep, overlaid by a thick sedimentary cover.

The present-day shortening across Outer Albanides has been documented by geodetic investigations; in the fixed Apulia Plate reference, velocities measured by GPS show a shortening across Outer Albanides with a 3–4 mm yr^{-1} NE–SW shortening rate (Jouanne *et al.* 2012; D'Agostino *et al.* 2020; see Fig. 4c in this paper) in Northern Albania to 4.9 mm yr^{-1} in Southern Albania (Jouanne *et al.* 2012). This spatial variation expresses a clockwise rotation of Albanides and northwestern Greece. The shortening rate increases to 8.9 mm yr^{-1} (directed NE–SW) according to Valkaniotis *et al.* (2020) in the region of Epirus (NW Greece).

1.2 Historical seismicity

During the 2500 yr, the city of Durrës has undergone strong earthquakes. Several studies (Sulstarova & Kociaj 1975; Aliaj *et al.* 2010,

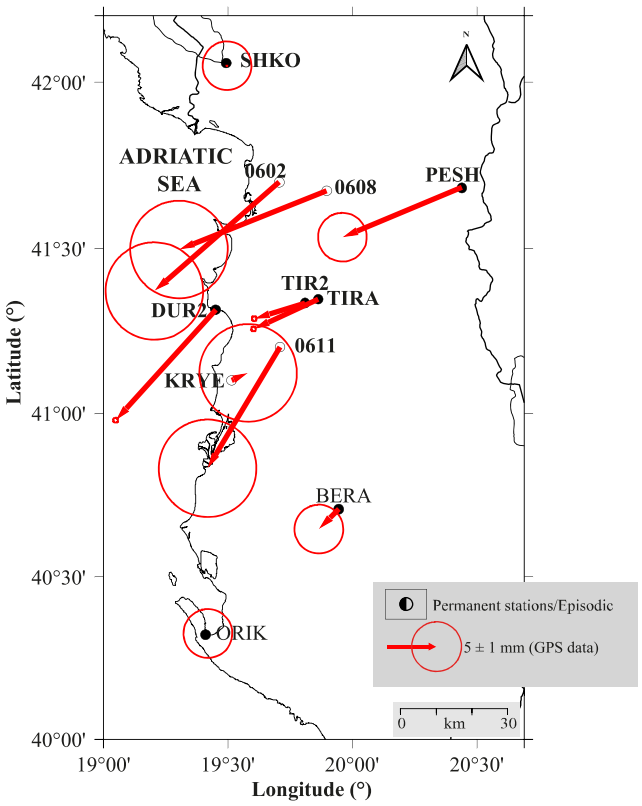

Figure 4. Map of the observed coseismic slip. The horizontal displacement for permanent GPS stations and campaign measurements (red arrows) with the 95 per cent error ellipses.

2012) state that Durrës was struck during the ancient times by several strong earthquakes; we can distinguish the 58 BC, 334 AD, 346 AD, 506 AD, 521, 1273, 1279 and 1870 earthquakes, which resulted in severe losses. The earthquakes of 334, 346 and 506 AD (maximum intensity IMAX = 8–9° [MSK-64]), the earthquake of 1273 (equivalent magnitude M_w 6.7 [EPICA; SHEEC, 1900–2020]) and 1926 (equivalent magnitude M_w 6.3 [SHEEC]) forced the abandonment of devastated Durrës city (Sulstarova & Koçiaj 1975; Stucchi *et al.* 2012; Storchak *et al.* 2015; Rovida & Antonucci 2021). The most significant seismic events in the area, that have affected the site of interest, are the 1617 Kruja earthquake (M_w 6.2; epicentre Intensity $I_o = 8$ [MSK-64]; the 26 August 1852 Rodoni Cape earthquake (M_w 6.2; epicentre Intensity $I_o = 8$ [MSK-64]; the 16 May 1860 Ndroqi earthquake (M_w 6.2); the 4 February 1934 Ndroqi earthquake (M_w 5.7); the 19 August 1970 Vrapi earthquake (M_w 5.6); the 16 September 1975 Rodoni Cape earthquake (M_w 5.4); the 9 January 1988 Tirana earthquake (M_w 5.9); the 21 September 2019 Durrës Earthquake (M_w 5.6) and the 26 November 2019 Durrës earthquake (M_w 6.4; Sulstarova & Koçiaj 1975; Sulstarova *et al.* 2003; Stucchi *et al.* 2012; Rovida & Antonucci 2021; Anton *et al.* 2022).

1.3 Instrumental seismicity

The first instrumental recorded earthquake located in Durrës was that which occurred on 17 December 1926 (M_w 6.4, although doubtful, as different values have been given: 6.2–6.4), with an epicentral intensity $I_0 = 9°$ (MSK-64; Aliaj *et al.* 2010, 2012). During the last two decades, several moderate earthquakes $M > 5.0$ have hit Durrës, mentioning the 5 September 2007 (4.8–5.0) and the 4 July 2018 (M_w 5.1) earthquakes. The last seismic activity, resulting in the strongest instrumental recorded seismic activity during the last four decades in this region, started on 21 September 2019 (M_w 5.6), located 3-km west of Shijak, subsequently followed, after 10 min, by an M_w 5.1 aftershock (Figs 2 and 3; Aliaj 2020; Papadopoulos *et al.* 2020; Mavroulis *et al.* 2021; Anton *et al.* 2022). The main shock and seismic sequence aftermath caused severe damage to local building environments. The sequence culminated with the strong shock of 26 November 2019 (M_w 6.4), preceded by several immediate foreshocks (M_w 2.0–4.4), followed by numerous aftershocks ($M_w > 5.0$; Fig. 3a).

To determine the seismic activity rate, we plot the spatiotemporal distribution (Figs 3a and b) of aftershocks and foreshocks that correspond to the area of the main shock. The location of the main shock varies with different agencies; the reason mentioned by Papadopoulos *et al.* (2020) was the lack of an appropriate velocity and structure model. We can also mention the lack of instrumentation in the epicentral area. The Albania Seismic network is composed of six seismic stations: TIR, PHP, SDA, BBA1, VLO and KBN. The nearest station to the earthquake epicentre is the Tirana station (TIR), 33 km east of Durrës, causing an erroneous location and undefined seismic depth. The Tirana (TIR) station is equipped with an STS-2 (VBB) sensor. The Peshkopia (PHP) broadband (BB) seismic station, located more than 100 km to the NE of the epicentre area, it operates at a frequency band of 0.033–50 Hz. The Shkodra (SDA) station, located around 60 km NNW of the epicentre area, is settled on limestones and equipped with a broad-band (BB) Guralp-40T (40 s) sensor, and it operates in the same frequency range as the PHP station. Over 100 km away from the epicentral area, three more stations could detect and record the earthquake: the Vlora (VLO) station located S, the Korca (KBN) seismic station located SE and the BBA1 deployed into Marinza oilfield (Métois *et al.* 2020) (see Appendix A, Fig. A1). The temporal distribution of magnitude (Fig. 3c) and the fitting of the Gutenberg–Richter law to cumulative number of events versus magnitude curbe (Gutenberg & Richter 1956; Mignan, Woessner 2012) suggest a magnitude of completeness for the Institute of GeoSciences (IGEO) (https://geo.edu.al) catalogue of $M_L = 2.8$ (Fig. 3d). We considered all events of magnitude $2.8 \leq M_L \leq 6.4$ for the period between 2018 and 1 January 2021.

2 DATA ANALYSIS

2.1 GNSS data analysis

We analysed data from campaign and permanent GNSS stations together with continuous GNSS data from the GNSS sites defined in the IGb14 reference frame (ftp://igs-rf.ign.fr/pub/IGb14) [AJAC (Ajaccio, France), BRST (Brest, France), EBRE (Roquetes, Spain), GANP (Ganovce-Poprad, Slovakia), GLSV (Kiev, Ukraine), GRAS (Caussols, France), GRAZ (Graz, Austria), MAS1 (Maspalomas, Spain), MAT1 (Matera, Italy), MATE (Matera, Italy), MEDI (Medicina, Italy), NICO (Nicosia, Cyprus), RABT (Rabat, Maroc), RAMO (Mitzpe Ramon, Israel), SFER (San Fernando, Spain), SOFI (Sofia, Bulgaria), TLSE (Toulouse, France), UZHL (Uzhgorod, Ukraine), ZECK (Zelenchukskaya, Rusia), ZIM2 (Zimmerwald, Switzerland) and ZIMM (Zimmerwald, Switzerland)] (ftp://ftp.epncb.oma.be/pub/obs/). Data were analysed using Bernese 5.2 software (Dach *et al.* 2015) with absolute antenna phase centre offset models, precise orbits, Earth rotation parameters and ocean and atmospheric tidal loading estimates. Velocities and time-series

Table 1. Focal mechanisms of 26 November 2019, 02:54 UTC earthquake by different sources.

Institute	Strike (°)	Rake (°)	Dip (°)	Strike (°)	Rake (°)	Dip (°)	Depth (km)	M_w
GFZ (1)	151	89	72	335	94	18	26	6.4
GCMT (2)	145	79	68	351	114	25	24.1	6.4
USGS (3)	156	89	63	338	92	27	19.5	6.4
CPPT (4)	168	104	69	312	57	25	15	6.4
INGV (5)	134	84	82	350	126	10	21	6.2
AUTH (6)	150	109	49	303	69	44	6	6.1

Sources: 1. GFZ (https://geofon.gfpotsdam.de/old/data/alerts/2019/gfz2019xdig/mt.txt); 2. GCMT (https://www.globalcmt.org/CMTsearch.html); 3. USGS (https://earthquake.usgs.gov/earthquakes/eventpage/us70006d0m/moment-tensor); 4. CPPT (https://www.emsccsem.org/Earthquake/mtfull.php?id=807751andyear=2019;INFO; 5. INGV (http://cnt.rm.ingv.it/en/event/23487611/?tab=MeccanismoFocale#TDMTinfo), 6. AUTH (http://geophysics.geo.auth.gr/ss/); 7. EMSC (https://www.emsccsem.org/Earthquake/earthquake.php?id=807751).

Table 2. GPS stations for different agencies used in this study.

Agencie	Station	Lat.	Long.	Elevation (m)	Operational time
ALBPOS	DUR2	41.3155	19.4510	63.45	2008–2020
	TIR2	41.3356	19.8095	170.80	2008–2020
IGEO	TIRA	41.3473	19.8632	236.87	Since 2002
	PESH	41.6848	20.4398	746.02	Since 2003
	BERA	40.7082	19.9455	269.25	Since 2005
	ORIK	40.3272	19.4198	42.30	Since 2017
	SHKO	42.0506	19.4963	66.89	Since 2002
	HIMA	40.0888	19.7582	179.00	Since 2014
	KRYE	41.1014	19.5148	169.62	Permanent station since December 2019
	KULL	41.2541	19.3312	46.00	Permanent station since December 2019
Campaign points (IGEO&ISTerre)	KRYE	41.1014	19.5148	169.62	2006, 2009, 2017, 2019
	0602	41.7006	19.7056	120.29	2006, 2009, 2017, 2019
	0608	41.6750	19.8965	256.32	2006, 2009, 2017, 2019
	0611	41.2026	19.7097	149.61	2006, 2009, 2017, 2019
ASIG	DIV3	41.0074	19.5617	120.36	Since January 2020
	DUR3	41.4097	19.3970	47.34	
	ELB3	41.1050	20.1025	229.17	
	FIE3	40.6970	19.5397	123.52	
	GRA3	40.8674	20.1879	292.45	
	KOR3	40.6204	20.7389	877.69	
	LES3	40.1499	20.5989	953.37	
	LIB3	41.1851	20.3215	388.69	
	ORI3	40.3271	19.4197	40.64	
	PER3	40.2331	20.3531	294.51	
	PESH	41.6848	20.4398	746.06	
	POG3	40.8844	20.6994	750.46	
	PUK3	42.0447	19.9035	849.02	
	RRE3	41.7679	19.8749	142.49	
	SHE3	41.8120	19.5853	44.78	
	SHK3	42.0505	19.4963	67.82	
	TEP3	40.2948	20.0143	308.49	
	TIR3	41.3208	19.8506	257.88	

were estimated in the IGb14 reference frame with discontinuities associated with this reference frame (ftp://igs-rf.ign.fr/pub/IGb14).

In this study, we analysed permanent GNSS data (Table 2) of stations belonging to the IGEO network, stations belonging to the Albanian State Authority for Geoinformation (ASIG) network, operational since 1 January 2020 (from 2020 to 2021) and the ALBPOS network (operational from 2009 to the end of 2019) (GNSS Network of Albania, 2017). Both IGEO and ASIG GNSS permanent stations are installed on concrete geodetic pillars built on stable outcrops. We also analysed campaign GNSS measurements we made in 2003, 2006, 2008, 2009, 2017 and December 2019.

In the time-series of the permanent GNSS stations, we examined the existence of outliers, periodic functions, discontinuities and velocity changes after these events, using the FODITS program (Ostini *et al.* 2008, 2010; Ostini 2012), which is embedded in the Bernese 5.2 software. This analysis allows to conclude at the lack of significant annual and semi-annual signals in the studied time-series and the lack of discontinuities for permanent Albanian stations.

Table 3. Coseismic displacement estimated for 26 November 2019, earthquake at the campaign GNSS measurements 0602, 0608, 0611, KRYE, and ALBPOS DUR2, TIRA, TIR2, PESH and BERA (Fig. 4).

Station	Lat.	Long.	Elevation (m)	East (mm)	North (mm)	Up (mm)
0602	41.7006	19.7056	120.29	-12.5 ± 2	-10.9 ± 2	-7.1 ± 10
0608	41.6750	19.8965	256.32	-14.8 ± 2	-5.9 ± 2	33.9 ± 10
0611	41.2026	19.7097	149.61	-7.3 ± 2	-12.2 ± 2	40.0 ± 10
KRYE	41.1014	19.5148	169.62	1.7 ± 2	0.7 ± 2	-0.8 ± 10
DUR2	41.3155	19.4510	63.45	-10.1 ± 0.1	-11.1 ± 1	-2.3 ± 10
TIRA	41.3473	19.8632	236.87	-6.5 ± 0.1	-2.9 ± 0.1	-4.5 ± 10
TIR2	41.3356	19.8095	170.80	-5.1 ± 0.1	-1.6 ± 0.1	-2.7 ± 10
PESH	41.68 476	20.43 976	746.02	-12 ± 1	-5 ± 1	0 ± 10
BERA	40.70 816	19.94 546	269.25	-2 ± 1	-2 ± 1	-3 ± 10
ORIK	40.3272	19.4198	42	0 ± 1	0 ± 1	0 ± 10
SHKO	42.0506	19.4963	67	0 ± 1	0 ± 1	0 ± 10

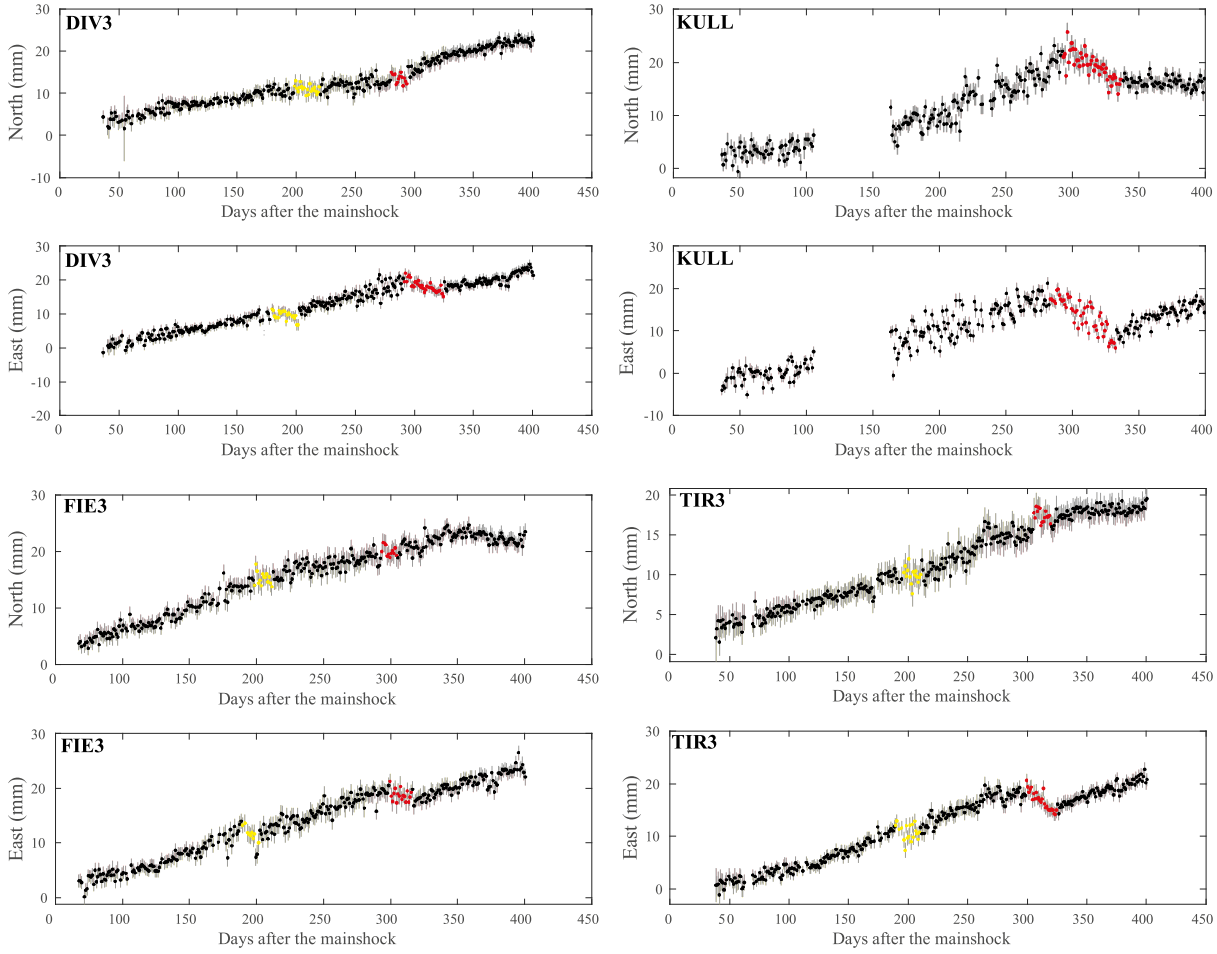

Figure 5. Time-series of horizontal components (North, East component) measured at stations DIV3, KULL, FIE3 and TIR3. The figures show the trending time evolution of displacement. The occurrence of SSE for + 200 events (yellow) and + 300 events (red).

2.1.1 Coseismic slip estimation

The GNSS measurements performed before and after the earthquake, both on campaign (Table 2) and permanent points (Table 2), allowed the quantification of the coseismic displacements associated with the main shock (Fig. 4). To calculate coseismic slip for GPS stations, we used nine stations (Table 3), from which four were measured during campaigns, and six were permanent stations (see Appendix B, Fig. B1). For campaign points, extrapolation of time-series until the day of the main shock is performed using interseismic velocities estimated in the IGb14 reference frame. Coseismic slip for campaign measurements was estimated by the difference between the extrapolated position value for the day of the main shock and the position measured after the earthquake.

2.1.2 GNSS time-series analysis

We studied the time-series of permanent station recordings after the earthquake. GNSS time-series have been expressed in the IGb14 reference frame (Fig. 5, see Appendix B, Fig. B2). Owing to the shutdown of the ALBPOS network just after the main shock, the

Table 4. Displacements estimated for the day + 200 SSE.

Station	Lat. (°)	Long. (°)	Elevation (m)	East (mm)	North (mm)	Duration (days after main shock)
DIV3	41.0074	19.5617	120.36	−0.7 ± 2	−0.98 ± 1	185 to 218
DUR3	41.4097	19.3970	47.34	−2.2 ± 2	−0.5 ± 1	191 to 204
ELB3	41.1050	20.1025	229.17	−1.6 ± 2.6	0 ± 1	180 to 206
FIE3	40.6970	19.5397	123.52	−2.3 ± 2	−1.1 ± 2	191 to 219
HIMA	40.0888	19.7582	179.00	−2.8 ± 2	0 ± 2	193 to 207
KRYE	41.1014	19.5148	169.62	−4.4 ± 2	−3.11 ± 2	183 to 226
PESH	41.6848	20.4398	746.06	−0.4 ± 2	0 ± 2	197 to 206
TIR3	41.3208	19.8506	257.88	−2.4 ± 2	−2.7 ± 2	180 to 213
TIRA	41.3473	19.8632	236.87	−4.1 ± 3	−2.3 ± 3	174 to 220
SHE3	41.8120	19.5853	44.78	−2.7 ± 1.5	0 ± 1.7	195 to 205
SHK3	42.0505	19.4963	67.82	−1 ± 1.5	−2.15 ± 2	176 to 215

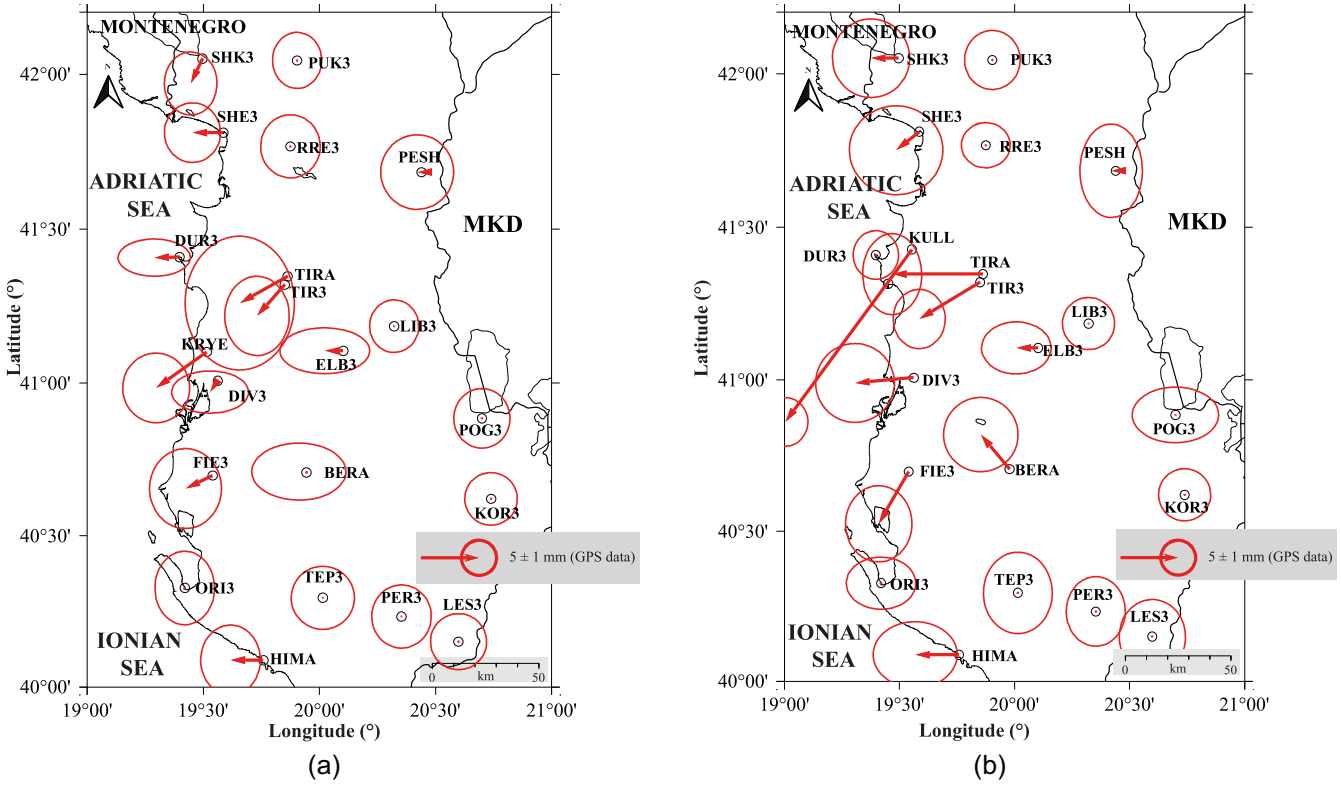

Figure 6 (a) Displacements associated with SSE (red arrows) occurring 200 d after 26 November 2019, Durrës earthquake with 1σ error ellipses. (b) Displacements associated SSE (red arrows) occurring 300 d after 26 November 2019, Durrës earthquake with 1σ error ellipses.

Table 5. Displacements estimated for the day + 300 SSE.

merStation	Lat.	Long.	Elevation (m)	East (mm)	North (mm)	Duration (days after main shock)
BERA	40.7082	19.9455	269.25	−2.5 ± 2	−3.06 ± 2	296 to 332
DIV3	41.0073	19.5616	120.36	−5.1 ± 2	−4.6 ± 2	290 to 322
ELB3	41.1049	20.1024	229.17	−1.9 ± 2	0 ± 1.5	312 to 321
FIE3	40.6969	19.5397	123.52	−2.6 ± 2	−4.5 ± 2	296 to 319
KULL	41.4281	19.5534	46.00	−11 ± 2	−15 ± 2	281 to 338
PESH	41.6847	20.4397	746.06	−0.4 ± 2	0 ± 2	295 to 318
SHE3	41.8120	19.5852	44.78	−2 ± 2	−1.62 ± 2	296 to 327
TIR3	41.3208	19.8506	257.88	−5.3 ± 2	−3.2 ± 2	299 to 323
TIRA	41.3473	19.8632	236.87	−7.9 ± 3	0 ± 2	273 to 307
SHK3	42.0505	19.4962	746.06	−2.4 ± 2	0 ± 2	302 to 322
HIMA	40.0888	19.7582	179.00	−3.8 ± 2	0 ± 2	295 to 323

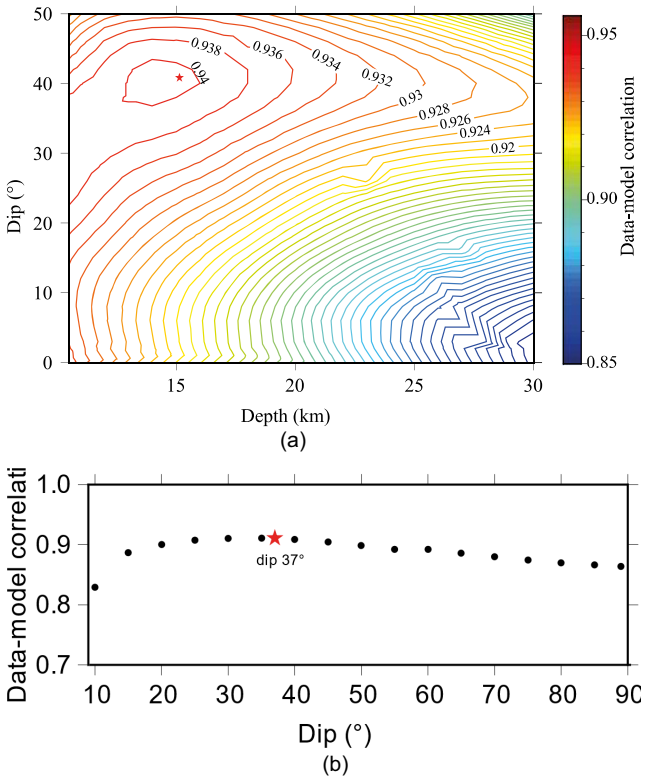

Figure 7 (a) Data–model correlation plot for depth between 10 and 30 km and dip angle between 0° and 50°. The optimal solution for the coseismic slip released during the main shock is obtained for a fault with the upper limit at 15-km depth and a 40° dip angle. (b) Data–model correlation plot for searching for the optimal solution to the second hypothesis. The optimal solution is obtained for a 37° dip angle but corresponds to a weak data–model correlation of 91.11 per cent, with a maximum slip of 0.4 m and a moment magnitude of M_w 6.26.

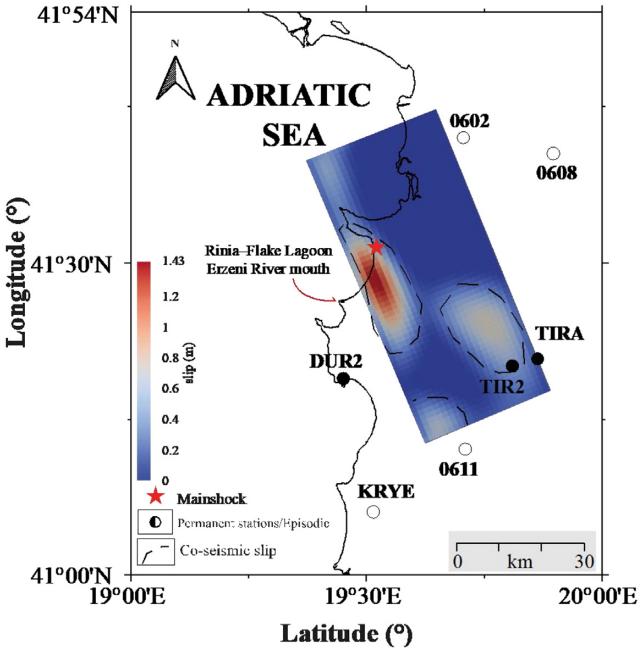

Figure 8. Coseismic slip distribution on a fault plane 56-km long, 25-km wide, 15-km deep and 40° dipping NE, estimated using InSAR data from three tracks—ascending 073 track, ascending 175, and descending 153—and GPS displacements (permanent and campaign GNSS measurements drawn by dots) (see Table 2). The dotted black line represents the coseismic patch corresponding to a maximum slip of 1.43 m and a moment magnitude of M_w 6.55.

post-seismic deformation following the main shock is poorly documented, as the ASIG stations taking over from the ALBPOS network did not start their measurements until early 2020. The only station that operated immediately after the main shock was the TIRA station, whereas the KULL station started in mid-December 2019. The time-series do not show a clear post-seismic signal, suggesting that most post-seismic deformation lasted a few weeks. Moreover, the GNSS time-series of stations in Albania showed velocity changes around day + 200 (DIV3, DUR3, ELB3, FIE3, HIMA, KEYE, PESH, TIR3, TIRA, SHE3 and SHK3) and day + 300 (BERA, DIV3, ELB3, FIE3, HIMA, KULL, PESH, SHE3, TIR3, TIRA and SHK3) after the main shock during 26 and 28 d, respectively (Fig. 5, see Appendix B, Fig. B2). We interpret these velocity changes as the occurrence of transient events interpreted as slow slip events (SSEs).

SSEs show variation in duration and horizontal displacement amplitude (from 174 to 226 d after the main shock for days + 200 SSE and from 273 to 338 d after the main shock for days 300 + SSE). We smoothed the cumulative displacement time-series to determine the SSE duration with a smooth coefficient of 0.1. The estimated SSE amplitude is the difference between the linear interpolations of the cumulative displacement time-series before and after SSE, for the same amount of days as the duration of SSE, according to the GNSS station. The associated error is the quadratic sum of the slope's standard deviations before and after SSE.

Maximum amplitudes associated with the day + 200 SSEs are observed on KRYE, TIRA and TIR3 time-series (Table 4 and Fig. 6a) with a maximum observed on the KRYE time-series (4.4 mm west, 3.11 mm south). It must be noticed that, unfortunately, there is a gap of data for this station around the day + 200 (see Appendix B, Fig. B2). Maximum amplitudes associated with the day + 300 SSEs are observed on KULL, TIR3, DIV3, and TIRA time-series (Table 5 and Fig. 6b) with a maximum observed on the KULL time-series (11 mm west, 15 mm south).

2.2 Coseismic interferograms with sentinel-1 data

We processed C-band Sentinel-1 SAR data spanning 26 November 2019, Durrës main shock. The epicentral area is covered by two ascending tracks (A073 and A175) and one descending track (D153), where images are acquired systematically every 6 d. For each track, using the NSBAS processing chain (Doin *et al.* 2011; Grandin 2015), we processed a time-series of deformation using all images acquired between 1 August 2019 and 7 February 2020, representing ∼30 images per track. We defined a redundant small-baseline network of interferograms from these images, including ∼140 interferograms per track. Before unwrapping, we corrected atmospheric phase delays using ERA-5 meteorological reanalysis, following Jolivet *et al.* (2011). We corrected the remaining stratified atmospheric delays by fitting a topography-correlated phase screen for each acquisition, with parameters of the correction fixed after an inversion in the interferometric network. After unwrapping and referencing all interferograms to a stable point (assumed to be located in a coherent area corresponding to the city of Tirana), we computed a time-series of ground displacement for each track to

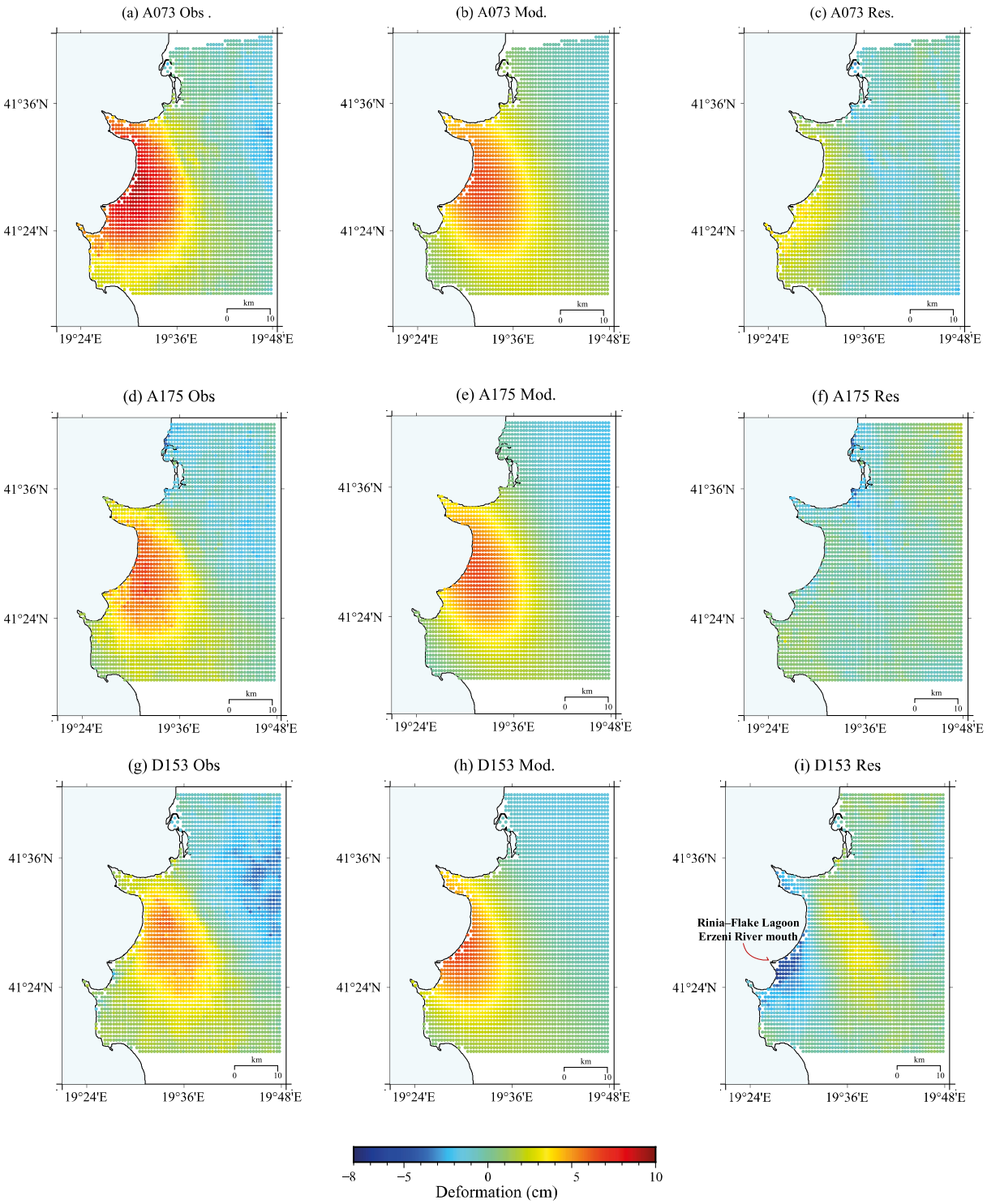

Figure 9. The first column represents the sampled InSAR data (a, d and g), the second column represents the displacements simulated by the optimal model (b, e and h). In contrast, the third column represents the residuals (observed-simulated displacements) (c, e and i).

separate the long-term deformation from the erratic contribution of atmospheric turbulence and jointly estimated a coseismic step at the time of the earthquake. Residual atmospheric delays in the resulting coseismic maps were mitigated by masking the deformation area and iteratively removing a phase-to-topography linear correlation and a low-order planar ramp. Finally, uncertainties were estimated by computing semi-variograms of the resulting coseismic InSAR maps, fitted with an exponential model whose parameters were extracted and injected into the covariance matrix in the subsequent inversion.

3 MODELLING

To model the coseismic slip distribution on the fault, we used the steepest descent method (SDM) software (Wang *et al.* 2009, 2011, 2012). This software is based on an iterative algorithm used for constrained least-squares optimization. It allows us to model the slip distribution on a rectangular fault separated into small rectangular pixels with a surface defined by patch value. Further, the SDM software can determine the offset between different datasets. The final model is a smooth slip model modelled with a 0.25 smoothing factor, which allows the minimization of misfit to data.

3.1 Modelling the coseismic slip

For modelling the coseismic deformation, we looked for the fault on which the earthquake occurred by searching for the optimal agreement between observations (coseismic displacement and early post-seismic deformation measured by GNSS and InSAR) and the model. The published focal solutions (Fig. 3, sources GFZ, GCMT, USGS, CPPT, INGV and AUTH) led us to test two hypotheses, a thrust dipping eastward, as proposed by Caporali *et al.* (2020), Ganas *et al.* (2020), Papadopoulos *et al.* (2020) and Moshou *et al.* (2019), and a steeply dipping back thrust—the Kashar–Preze–Rodon back thrust—that could end at the surface just east of the Preza monoclinal, as proposed by Govorčin *et al.* (2020).

We looked for the optimal model corresponding to the first hypothesis by conducting systematic research by varying the depth and dip angle of the fault. We assumed only an orientation N160° of the active thrust corresponding at the orientation of this fault given by focal mechanisms (Fig. 2). For the second hypothesis, assuming that the earthquake occurred along a known back thrust, we assumed that this fault arrives at the surface east of the Preza fold (Fig. 1). Therefore, we looked for the optimal solution by varying only its dip angle because its location is known.

The first hypothesis was tested for different combinations of depth and dip angle for fixed-width (25 km); length (56 km); average strike (160°); rake range [60°, 120°] and rectangular patches of ∼1 × 1 km^2.

The second hypothesis tested for a varying dip angle [10°, 89°] for fixed-width 25 km; length 40 km; average strike (150°); rake range [60°, 120°] and rectangular patches of ∼1 × 1 km^2. The optimal solution was taken for a dip equal to 37° ± 2° (Fig. 7b).

As shown in Figs 7(a) and (b), we obtained the optimal correlation between data and model for an earthquake localized along a thrust (first hypothesis) with a 94.5 per cent correlation (Fig. 7a). The second hypothesis can be rejected, considering the weak data–model correlation (Fig. 7b).

We consider that the optimal solution among the tested solutions is a thrust localized at a 15-km depth with a 40° dip angle (Fig. 8). This depth indicates that the earthquake probably occurred in the upper part of the basement, below the detachment layer of Outer Albanides.

Our preferred solution indicates coseismic slips concentrated near the main shock epicentre, with a 1.43-m maximum slip. If we consider only the patches near DUR2 (Fig. 8), corresponding to the epicentre of the earthquake, the corresponding moment magnitude (estimated using a rigidity coefficient of 3×10^{10} N m^2 for 369 patches with a surface of 10^6 m^2) is M_w 6.38; if we consider all patches, we determine a M_w 6.5. The moment magnitude M_w 6.38 agrees with the moment magnitude proposed by agencies and other scholars (Fig. 3 and agencies ref). The correlation (Fig. 7a) and the residual plots (Fig. 10) show a good agreement between the data and the model. Residuals reach 1 cm for campaign GNSS measurements (Fig. 10, green arrows) and 3 mm for permanent stations (Fig. 10).

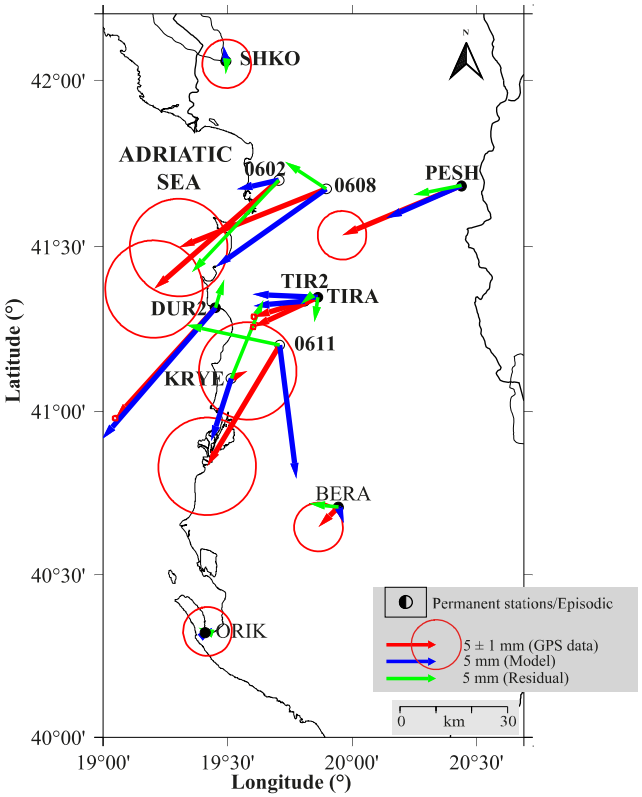

Figure 10. Coseismic slip, estimated using the time-series of the permanent GPS stations and campaigns (red arrows) with 95 per cent confidence ellipses; coseismic slip predicted by the optimal model (blue arrows), and residuals (green arrows).

The residuals for InSAR data for ascending A073 and A175 tracks do not pass 5 cm (Figs 9a–f). They show a good fit between the model and data; however, the descending D153 track displays unmodelled displacements in the Rinia–Flake Lagoon and Erzeni River mouth area, with residuals greater than 5 cm (Figs 9g–i). Referring to Lekkas *et al.* (2019), this area this area has been subjected to coseismic liquefaction with the ejection of liquefied material, formation of sand boils and lateral spreading. This phenomenon is controlled by shallow water levels and soft and unconsolidated lagoon sediments. We can propose that this area with important residuals reflects the occurrence of liquefaction 7.6-km southeast of the main shock.

We performed checkerboard tests to examine the resolution of our model (see Appendix C, Figs C1a–b, Fig. C2a–b and Figs C3a–b). We produced synthetic displacements for both GNSS and INSAR data using the GTdef software (Chen *et al.* 2009; Murekezi *et al.* 2020). Using these synthetic displacements, we used the SDM software to identify the patches introduced in our synthetic forward models and then to compare the output slip distributions.

The test considered six patches with a reverse slip of 1 m and six patches with 0 m displacement (see Appendix C, Fig. C1. a) on the fault located between 0 and 23 km in depth. The SDM software could accurately reproduce the patches (location and slip amplitude) when it is located at 0–7 km depth (see Appendix C, Fig. C1b), however, it did not precisely reproduce the patches when they are located deeper (see Appendix C, Fig. C1b).

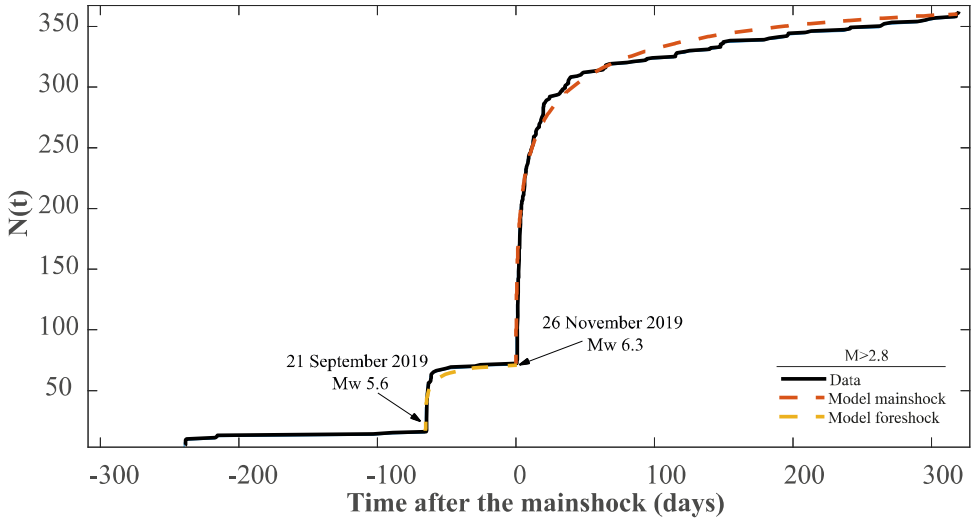

Figure 11. Time distribution of the cumulative number of aftershocks (blue line) with magnitude $M_L \geq 2.8$, from 1 March 2019 to 17 November 2020. The fit with Perfettini and Avouac's model is done for the M_w 5.8 foreshock on 21 September 2019 (yellow dashed line) and for the M_w 6.3 on 26 November 2019 earthquake (orange dashed line). The parameters obtained for the foreshock are $t_r = 34$ days and $d = 2006$ and main shock are $t_r = 179$ days and $d = 1037$ with $R_0 = 0.238$ events per day. R_0 was obtained from the microseismicity catalogue for events $M_L > 2.8$ before the foreshock.

To test the detection of a single patch, like our coseismic slip distribution, we performed also two tests considering a rectangular patch with a 1 m reverse slip (see Appendix C; Fig. C2a and Fig. C3a) using the geometric parameters of our best model. On the first test the patch is located in the same depth range as our best model (15–20 km depth; Appendix C; Fig. C2a) and the second test the patch is located deeper (20–25 km depth; see Appendix C, Fig. C2a).

We can conclude that, in this case, the SDM software could accurately reproduce the patch (location and slip amplitude) when it is located at 15–17 km depth (see Appendix C, Figs C1b and C2b). however, it did not precisely reproduce the patch when this one is located deeper (see Appendix C, Figs C1b and C3b). Thus, the SDM software has then a better resolution when the source is at located between the surface and 20 km depth. Since our best model slip is located at a depth of 15–20 km depth, we can suppose that it is well located and that the slip distribution is well described.

3.2 Post-seismic deformation

We analysed the evolution of the cumulative number of aftershocks over time using the model proposed by Perfettini & Avouac (2004). We aimed to analyse the possible post-seismic deformation. It was poorly documented by GNSS data, given the cessation of the ALBPOS network at the end of November 2019 and the start of the ASIG network in early 2020, leaving the post-seismic deformation likely to have occurred following the Durrës earthquake very poorly documented.

This model assumes that the post-seismic response of the medium surrounding the fault (the brittle creep section) drives the seismic activity after the main shock, following a strain–stress law. According to Perfettini and Avouac's model, we need to compare the time evolution of post-seismic and the aftershock's decay in time. Referring to this model, the cumulative number of aftershocks $N(t)$ time evolution follows an exponential distribution, given by the following equation:

$$N\ (t) = N\,(t\ =\ 0) + R_0 t_r \log\left(1 + d\left(\exp\left(\frac{t}{t_r}\right) - 1\right)\right) \qquad (1)$$

where $N(t\ =\ 0)$ denotes the cumulative number of earthquakes at time $t\ =\ 0$; R_0 denotes the seismicity rate before seismic activity rose. The d-parameter is related to the seismicity rate before and after any stress step, so this parameter is related to stress changes. It is the rate between those two values, and t_r is the characteristic time or the period needed for the seismicity rate to return to the initial rate R_0 (Perfettini & Avouac 2004). As the completeness magnitude of the IGEO catalogue is M_L 2.8 (Figs 3c and d), we considered only the magnitudes ($M_L \geq 2.8$). Perfettini and Avouac's model shows a good fit for 18 d after the foreshock and 50 d after the main shock but not for the full-time evolution of aftershocks. We propose a modification of Perfettini and Avouac's model, adding a new term $-R_0 t$ to take in to account the interseismic seismicity rate contribution, as shown in eq. (2).

$$N\ (t) = N\,(t\ =\ 0) + R_0 t_r \log\left(1 + d\left(\exp\left(\frac{t}{t_r}\right) - 1\right)\right) - R_0 t. \qquad (2)$$

The area selected to test the correspondence between the model and catalogue of aftershocks is shown in Fig. 3(b). Over 350 aftershocks followed the main shock, and the catalogue includes events from the end of 2018 till 1 January 2021.

Assuming a close relationship between the post-seismic deformation supposed to be controlled by afterslip and the temporal evolution of the cumulative number of aftershocks (Fig. 11, IGEO). The time evolution of the cumulative number of aftershocks (Fig. 11) highlights that most afterslip deformation occurs in the first month after the main shock. This would explain why the GNSS time-series do not show a marked exponential decay; most stations started their acquisitions 40 d after the earthquake. TIRA operating just after the earthquake is probably too far from the region undergoing post-seismic deformation to record this exponential decay.

3.3 SSE modelling

The GNSS time-series shows the occurrence of several SSEs, two at the day + 200 and the other around day + 300 can be easily characterized on several time-series (Fig. 5, see Appendix B,

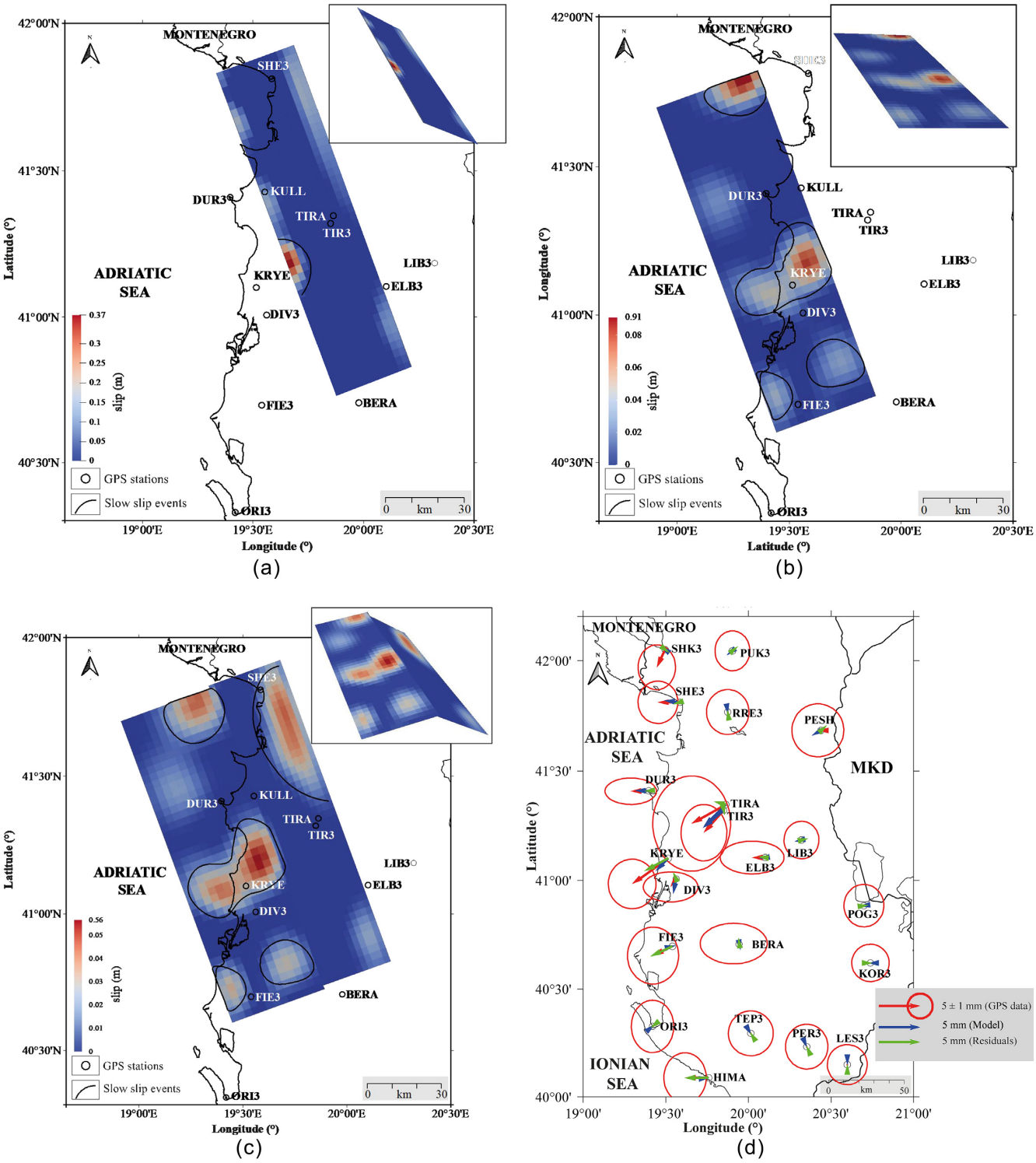

Figure 12 (a) Modelling of day + 200 SSE. The hypothesis of SSE localized along the basement thrust affected by the main shock. (b) Modelling of day + 200 SSE. The hypothesis of SSE localized along the detachment layer of Outer Albanides. (c) Modelling of day + 200 SSE. The hypothesis of SSE localized along the basal thrust and detachment layer of Outer Albanides. (d) Modelling of day + 200 SSE. Observed and predicted displacements and residuals for the hypothesis of SSE localized along the basal thrust. (e) Modelling of day + 200 SSE. Observed and predicted displacements and residuals for the hypothesis of SSE localized along the detachment layer of Outer Albanides. (f) Modelling of day + 200 SSE. Observed and predicted displacements and residuals for the hypothesis of SSE localized along the basal thrust and detachment layer of Outer Albanides.

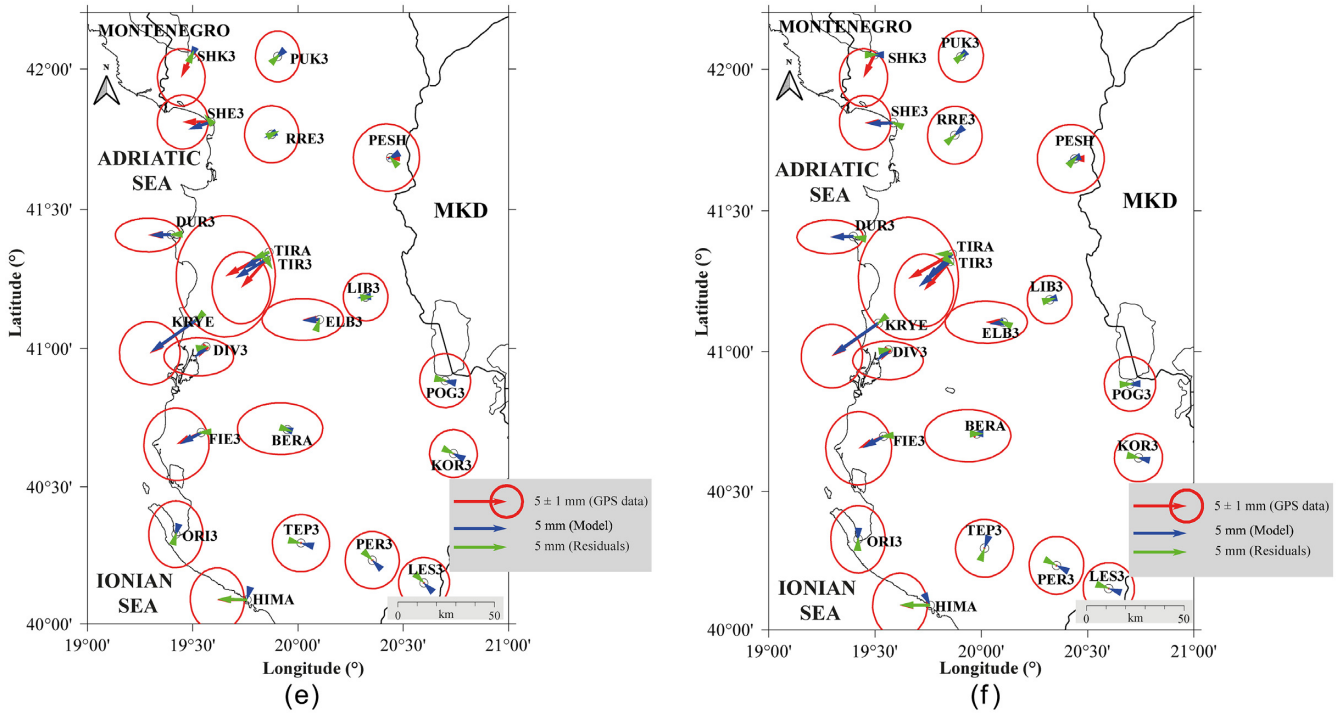

Figure 12 Continued.

Fig. B2), suggesting a regional extension of these events. Considering the structure of Outer Albanides and our result for the thrust responsible for the main shock (Fig. 1), we test three hypotheses: SSE along the coseismic thrust (Figs 12a and 14a), SSE along the detachment layer west of the coseismic slip (Figs 12b and 14b), and SSE along these two faults (Figs 12c and 14c). Table 6 lists the initial parameters of the hypotheses proposed and tested in this study.

Day + 200 SSE

The optimal solution for day + 200 SSE (Table 7) is obtained for the hypothesis of an SSE occurring along the detachment layer of Outer Albanides, modelled as a horizontal plane (maximum slip of 0.06 m) and along the basement thrust (maximum slip of 0.05 m) with an equivalent M_w of 6.22 for SSEs + 200 (Table 7, Figs 12c and f). The hypothesis of an SSE localized only along the basement thrust or along the detachment layer can be rejected due to the weak correlation between data and model (Table 7).

Day + 300 SSE

The optimal solution for day + 300 SSE (Table 8) is obtained for the hypothesis of an SSE occurring along the detachment layer of Outer Albanides modelled as a horizontal plane (maximum slip of 0. 41 m) and along the thrust affected by the main shock with an equivalent M_w of 6.24 (Table 8, Figs 13b and e). However, we can observe a small correlation change of 0.07 per cent between the correlation obtained for this hypothesis and that obtained for the model considering an SSE localized only along the detachment layer. Then, as our preferred model, we consider the model suggesting an SSE localized along the detachment layer of Outer Albanides formed by Triassic salt level (Figs 13a and d). The hypothesis that this SSE occurred only along the basement thrust affected by the main shock can be rejected.

4. DISCUSSION

4.1 Durrës earthquake

The geometry of our preferred model for the coseismic deformation is consistent with both the seismic profiles (Fig. 1) and tectonic cross-section [Fig. 14, Teloni *et al*. (2020) modified] of the Outer Albanides, comprising thrusts and back thrusts. We propose that the fault affected by the Durrës earthquake is a blind thrust at 15-km depth in the basement (Fig. 14). Most previous studies support this thrust hypothesis. This location agrees not only with Ganas *et al.* (2020), who proposed a 14-km fault depth thrust, but also with focal mechanisms proposed by different agencies (agencies ref; Fig. 2), suggesting a range of depths for this earthquake between 8 and 26 km. Our result is inconsistent with Govorčin *et al.*'s (2020) study that suggested that the earthquake took place along the Kashar–Preze–Rodon back thrust, dipping to the southwest. However, the dip of 40° we consider our optimal model is greater than those considered in other studies, which proposed a dip angle between 22° (Ganas *et al.* 2020), considering a uniform coseismic slip affecting a planar dislocation (using InSAR and GNSS data) and 18° (Caporali *et al*. 2020), using a dislocation model on an elastic half-space using InSAR data and permanent GNSS stations only. However, it remains in the range of the focal mechanism's 10–44° dip, where the maximum dip angle is proposed by AUTH of 44°.

In this study, the geometry of rupture proposed for the 26 November 2019 Durrës earthquake is close to the geometry proposed for the 1979 Montenegro earthquake localized in the same tectonic position in the Outer Dinarides fold-and-thrust belt (Anderson & Jackson 1987; Kuk *et al.* 2000; Pondrelli *et al.* 2006; D'Agostino *et al.* 2008; Schmitz *et al.* 2020). Most studies about the fault geometry

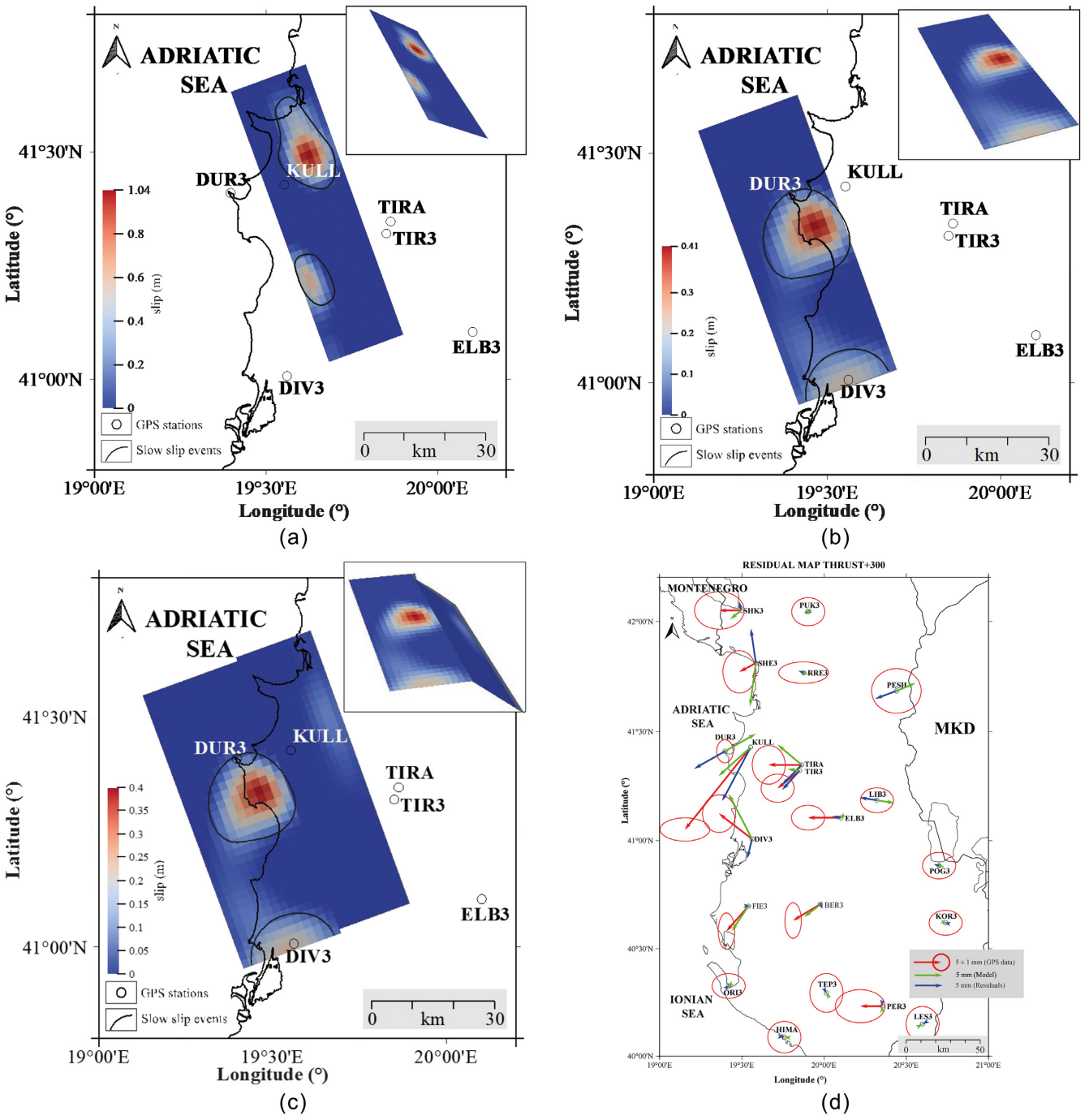

Figure 13 (a) Modelling of day + 300 SSE. The hypothesis of SSE localized along the basal thrust. (b) Modelling of day + 300 SSE. The hypothesis of SSE localized along the detachment layer of Outer Albanides. (c) Modelling of day + 300 SSE. The hypothesis of SSE localized along the basal thrust and the detachment layer of Outer Albanides (Upper Flat). (d) Modelling of day + 300 SSE. Observed and predicted displacements and residuals for the hypothesis of SSE localized along the basal thrust. (e) Modelling of day + 300 SSE. Observed and predicted displacements and residuals for the hypothesis of SSE localized the detachment layer of Outer Albanides. (f) Modelling of day + 300 SSE. Observed and predicted displacements and residuals for the hypothesis of SSE localized along the basal thrust and detachment layer of Outer Albanides.

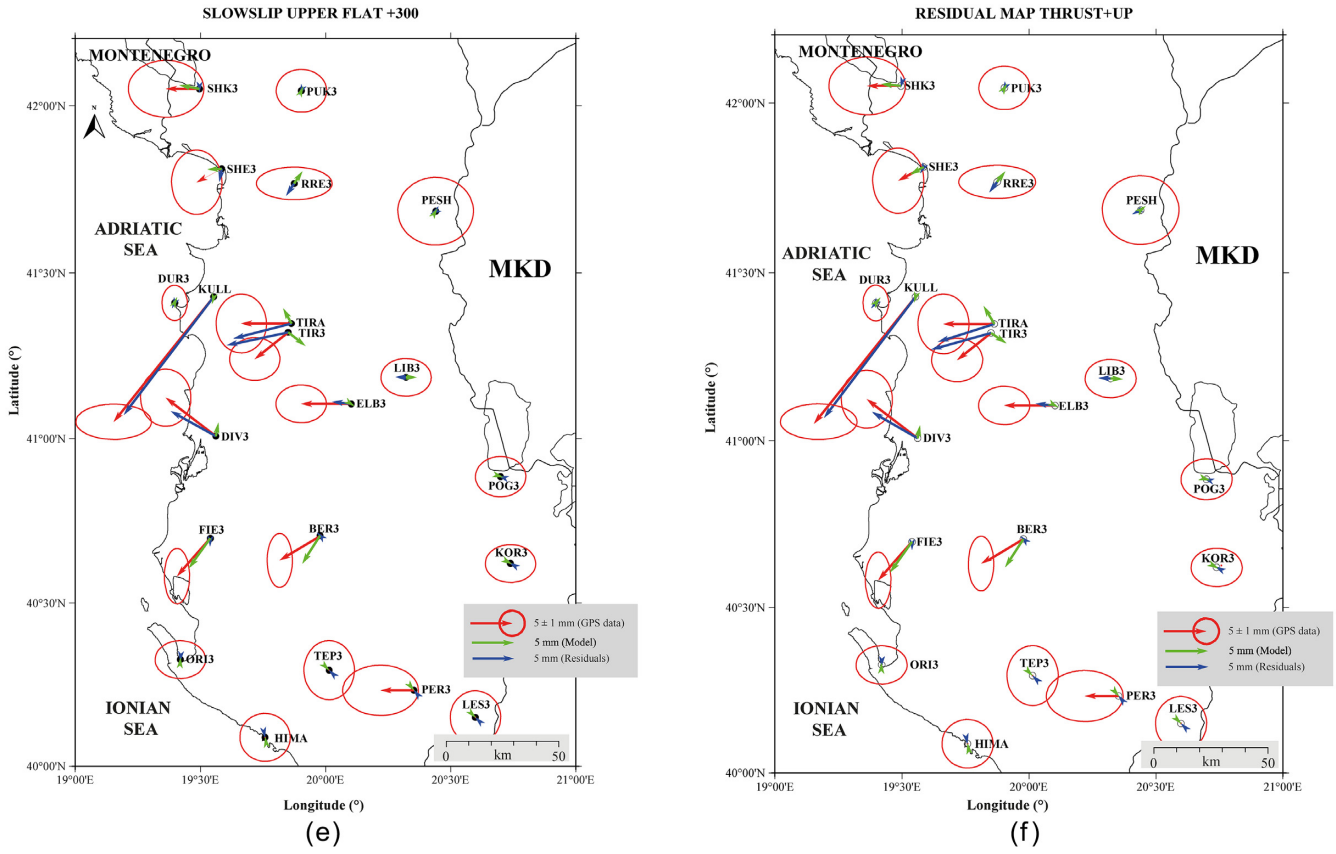

Figure 13 Continued.

of the 1979 Montenegro earthquake proposed a depth between 15 and 22 km dipping NE (Console & Favali 1981; Benetatos & Kiratzi 2006; Boore *et al.* 1981; Schmitz *et al.* 2020; Aliaj & Muço 1983; Sulstarova 1983). Meanwhile, Benetatos & Kiratzi (2006) proposed the earthquake occurred along a thrust parallel to the coastline, dipping to the NE (14°) at a 7-km depth. Considering that this last study proposed the most reliable location, geometry, and depth for the 1979 Montenegro earthquake, the main difference between this event and the 26 November 2019 Durrës earthquake would be the depth difference. The two earthquakes occurred probably along the most external basement ramp of the fold-and-thrust belt, suggesting an in-sequence deformation. The depth difference between these major earthquakes reflects the change between the Dinarides, involving a relatively thin sedimentary cover, and the northern part of Albanides, involving a thick sedimentary cover formed, as for the Dinarides by Mesozoic and Cenozoic formations, but also by very thick Miocene, Pliocene and Quaternary formations of the Periadriatic depression (Figs 1 and 14). The Lezha transfer strike-slip fault accommodates the change between these thin and thick skin tectonics of Albanides (Fig. 2).

4.2 Post-seismic deformation

Unfortunately, because of the lack of permanent GNSS stations operating for the month following the main shock, the exponential increase of displacement characteristic of post-seismic deformation cannot be detected on the GNSS time-series. Nevertheless, the evolution of the cumulative number of aftershocks suggests this deformation occurs 30–40 d after the main shocks. The installation of a new permanent GNSS network allows documenting deformation occurring after 2020.

4.3 Occurrence of SSEs

GNSS time-series allow for detecting the occurrence of two SSEs in numerous stations. The occurrence of SSE after a main shock in a collisional belt has rarely been documented in Hokkaido Island (Ohzono *et al.* 2014) and in Taiwan (Canitano *et al.* 2019; Li *et al.* 2020).

Most SSEs occur in subduction zones: Cascadia (Dragert *et al.* 2001; Miller *et al.* 2002; Rogers & Dragert 2003; Szeliga *et al.* 2004), Mexico (Lowry *et al.* 2001, 2006; Kostoglodov *et al.* 2003; Larson *et al.* 2004; Vergnolle *et al.* 2010; Radiguet *et al.* 2011), Alaska (Ohta *et al.* 2006), Japan (Hirose *et al.* 1999; Ozawa *et al.* 2002), New Zealand (Wallace *et al.* 2017) and Costa Rica (Protti *et al.* 2004; Brown *et al.* 2005).

Simulations of these SSE suggest their occurrence along the upper flat corresponding to the detachment layer of Outer Albanides or along the basement thrust and upper flat of Outer Albanides (Fig. 14). The upper flat corresponds to the efficient detachment layer formed by Triassic evaporites (salt, as observed in the Dumre diapir). Then, we can propose that these SSEs are controlled by the specific rheology of the salt, forming the detachment layer. The occurrence of SSE yields another interpretation of the seismic hazard (Thatcher 2001; Vergnolle *et al.* 2010) of the Durrës area.

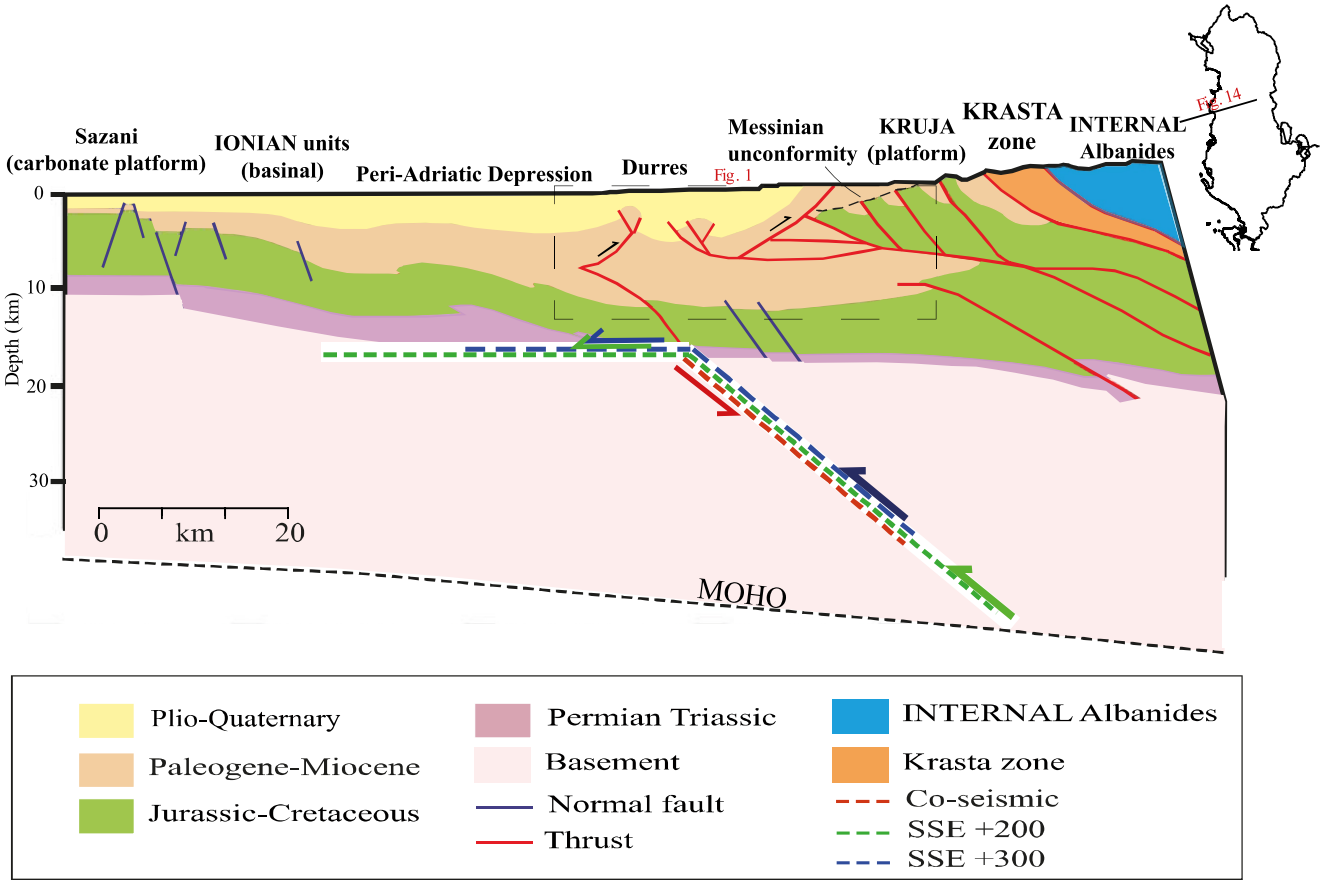

Figure 14. [from Telfoni *et al.* (2020), modified]. The white line represents our optimal model for coseismic slip, SSEs + 200 and + 300 slip distribution. The fault model for coseismic slip is a thrust fault with a 25-km width (red dashed line); the maximum coseismic slip is located around Durrës (red arrow). The SSEs for + 200 d occurred along the upper flat and basement thrust (green dashed line) with a larger width than the coseismic slip (green arrows). The SSEs for + 300 d occurred on the upper flat corresponding with the detachment layer of Outer Albanides (blue dashed line) with maximum slip occurrence around Durrës city (blue arrow).

Table 6. Fault geometry parameters of rectangular dislocations for the flat plane representing the Outer Albanides detachment layer (flat) and thrust.

Events	Fault	Strike (°)	Rake (°)	Dip (°)	Depth (km)	Width (km)	Length (km)
200+	Thrust	340	60–120	40	15	40	130
	Flat	340	60–120	0	15	40	130
300+	Thrust	340	60–120	40	15	25	70
	Flat	340	60–120	0	15	25	70

Table 7. Correlation between data and model for slow slip distribution of day + 200 SSE.

200+			
	Correlation	M_w	Maximum slip (m)
Upper flat	0.8749	6.08	0.09
Upper flat and thrust	0.8913	6.22	0.11
Thrust	0.7332	6.25	0.37

Table 8. Correlation between data and model for slow slip distribution of day + 300 SSE.

300+			
	Correlation	M_w	Maximum slip (m)
Upper flat	0.9644	6.24	0.41
Upper flat and thrust	0.9651	6.27	0.48
Thrust	0.7498	6.40	1.04

It highlights the need to consider the main earthquake followed by their post-seismic deformation and the SSE in the seismic budget that can delay or advance the occurrence (Thatcher 2001; Vergnolle *et al.* 2010) and the size reduction of the next earthquakes with the same magnitude (Correa-Mora *et al.* 2008; Vergnolle *et al.* 2010).

5 CONCLUSION

In this study, we propose a coseismic slip distribution for the M_w 6.4, 2019 Durrës earthquake using InSAR, permanent and campaign GNSS measurements. We find that this earthquake took place along a basement thrust with a 40° dip to the east, and top at 15 km depth. Our best model finds a coseismic slip reaching 1.4 m at a depth of

15 km with an associated magnitude of M_w 6.4. Our study allows rejecting the hypothesis of a rupture occurring along a back-thrust east of Durrës. The post-seismic deformation is not detected due to a lack of GNSS data during the month after the main shock. However, the distribution of aftershocks over time suggests that most of the post-seismic deformation took place in the month following the main shock. During the 18 months after the Durrës earthquake, we detected, for the first time in Albanides, the occurrence of two SSE in the GNSS time-series. We detect the first SSE approximately 200 d after the main shock with a duration of 26 d and a maximum amplitude of 4.4 mm on the east component and 3.1 mm on the north component, and the second SSE approximately 300 d after the main shock lasting 28 d and a maximum amplitude of 11 mm on east component and 15 mm on the north component.

If we assume that these two SSEs are located on faults associated with the Durrës earthquake, we find that they occurred on the detachment level of the Outer Albanides located west of the basement thrust affected by the Dürres earthquake or on both this detachment level and this basement thrust. These SSE are therefore one of the few examples of SSE within a fold and thrust belt.

ACKNOWLEDGMENTS

The campaign GNSS measurements in 2003, 2006, 2009, 2011 and 2019 were supported by SFP 977993 NATO, ISTerre, University Savoie Mont Blanc and Institute of Geosciences in Albania. We thank David Marsan for analysing the aftershock catalogue and his suggestions to improve the work and Marianne Métois and its ALBA Project to have funded the measurement of campaign points in 2017. We are grateful to Embassy of France in Albania for the scholarship attribution to Kristina Matraku.

DATA AVAILABILITY

The data underlying this paper are available in its online supplementary material and in Open Science Framework at osf.io/487pu.

REFERENCES

Aliaj, S. & Muço, B., 1983.The geological conditions that generated the earthquake of April 15, 1979, *Dev. Solid Earth Geophys,* **15,** 79–83.

Aliaj, Sh., 2012. Neotektonika e Shqiperisë, f. 210–231.

Aliaj, Sh., 2020. Seismotectonics of the Albanides Collision Zone: Geometry of the Underthrusting Adria Microplate Beneath the Albanides, *JNTS 2,* **JNTS,** 3–40.

Aliaj, Sh., Kociu, S., Muco, B. & Sulstarova, E., 2010. Seismicity, seismotectonics and seismic hazard assessment in Albania (In Albanian with English Extended Summary).

Anderson, H. & Jackson, J., 1987. Active tectonics of the Adriatic region, *Geophys. J. Int.,* **91,** 937–983.

Anton, A. *et al.*, 2022. EERI Earthquake Reconnaissance Report-M6.4 Albania Earthquake on November 26 2019, doi:10.13140/RG.2.2.15321.60008.

Bare, V., Mehillka, L., Skrame, J. & Çobo, L., 1996. The contribution of flattering for structural balancing in External Albanides, in *Proceedings of the1st Congress of the Balkan Geophysical Society,* Athens, Greece, September 2–27.

Benetatos, C. & Kiratzi, A., 2006. Finite-fault slip models for the 15 April 1979 (M-W 7.1) Montenegro earthquake and its strongest aftershock of 24 May 1979 (M-W 6.2), *Tectonophysics,* **421,** 129–143.

Biermanns, P., Schmitz, B., Ustaszewski, K. & Reicherter, K., 2019. Tectonic geomorphology and Quaternary landscape development in the Albania - Montenegro border region: an inventory, *Geomorphology,* **326,** 116–131.

Boore, D.M., Sims, J.D., Kanamori, H. & Harding, S., 1981. The Montenegro, Yugoslavia, earthquake of 15 April, 1979: source orientation and strength, *Phys. Earth planet. Inter.,* **27,** 133–142.

Brown, K.M., Tryon, M.D., DeShon, H.R., Dorman, L.M. & Schwartz, S.Y., 2005. Correlated transient fluid pulsing and seismic tremorin the Costa Rica subduction zone, *Earth planet. Sci. Lett.,* **238,** 189–203.

Canitano, A., Gonzalez-Huizar, H., Hsu, Y.-J., Lee, H.-M., Linde, A.T. & Sacks, S., 2019. Testing the influence of static and dynamic stress perturbations on the occurrence of a shallow, slow slip event in eastern Taiwan, *J. geophys. Res.,* **124,** 3073–3087.

Caporali, A., Floris, M., Chen, X., Nurce, B., Bertocco, M. & Zurutuza, J., 2020. The November 2019 Seismic Sequence in Albania: geodetic Constraints and Fault Interaction, *Remote Sens*., **12,** 846.

Chen, T., A.V. Newman, L., Feng, H. & Fritz, M., 2009. Slip distribution from the 1 April 2007 Solomon Islands Earthquake: a unique image of near-trench rupture, *Geophys. Res. Lett.,* **36**(16), doi:10.1029/2009GL039496.

Console, R. & Favali, P., 1981. Study of the Montenegro earthquake sequence (March–July 1979), *Bull. seism. Soc. Am.,* **71,** 1233–1248.

Correa-Mora, F., DeMets, C., Cabral-Cano, E., Diaz-Molina, O. & Marquez-Azua, B., 2008. Interplate coupling and transient slip along the subduction interface beneath Oaxaca, Mexico, *Geophys. J. Int.,* **175,** 269–290.

D'Agostino, N. *et al.*, 2020. Active crustal deformation and rotations in the southwestern Balkans from continuous GPS measurements, *Earth planet. Sci. Lett.,* **539,** doi:10.1016/j.epsl.2020.116246.

D'Agostino, N., Avallone, A., Cheloni, D., D'Anastasio, E., Mantenuto, S. & Selvaggi, G., 2008. Active tectonics of the Adriatic region from GPS and earthquake slip vectors, *J. geophys. Res.,* **113**(B12), doi:10.1029/2008JB005860.

Dach, R. Lutz, S., Walser, P. & Fridez P., 2015.Bernese GNSS Software Version 5.2. User manual, Astronomical Institute, University of Bern, Bern Open Publishing, doi:10.7892/boris.72297; ISBN: 978-3-906813-05-9.

Dalipi, H., 1985. The main phases of the geologic evaluation history of Outer Albanides (In Albanian), *Oil Gas J.,* **2,** 33–54.

Dhima, S., Misho, V. & Hajnaj, P., 1996. The seismic interpretation for exploration of new target in South Albania, in *Proceedings of the 1st Congress of the Balkan Geophysical Society,* Athens, Greece, September 2–27.

Doin, M.-P., Guillaso, S., Jolivet, R., Lasserre, C., Lodge, F., Ducret, G. & Grandin, R., 2011. Presentation of the small-baseline NSBAS processing chain on a case example: the Etna deformation monitoring from 2003 to 2010 using ENVISAT data, in *Proceedings of the European Space Agency Symposium ≪ Fringe ≫,* Frascati, Italy.

Dragert, G., Wang, K. & James, T., 2001. A silent slip event on the deeper Cascadia subduction interface. *Science (New York, N.Y.),* **292,** 1525–1528.

Frasheri, A., Bushati, S. & Bare, V., 2009. Geophysical outlook on structure of the Albanides. *J. Balkan Geophys. Soc.,* **12,** 9–30.

Frashëri, A., Nishani, P., Bushati, S. & Hyseni, A., 1996. Relationship between tectonic zones of the Albanides, based on results of geophysical studies. Peri Tethys Memoir 2: Structure and Prospects of Alpine Basins and Forelands, *Mém. Mus. Natn. Hist. nat.,* **170,** 485–511.

Ganas, A. *et al.*, 2020. Ground deformation and seismic fault model of the M6.4 Durrës (Albania) Nov. 26, 2019 earthquake, based on GNSS/INSAR observations. *Geosciences,* **10**(6), 210, https://www.mdpi.com/2076-3263/10/6/210/htm

Govorčin, M., Wdowinski, S., Matoš, B. & Funning, G.J., 2020. Geodetic source modeling of the 2019, Mw 6.3 Durrës, Albania earthquake: partial rupture of a blind reverse fault, *Geophys. Res. Lett.,* **47,** e2020GL088990.

Grandin, R., 2015. Interferometric processing of SLC Sentinel-1 TOPS data, in *Proceedings of the European Space Agency Symposium ≪ Fringe ≫,* Frascati, Italy.

Guri, S. & Guri, M., 1996. The seismic contribution on interpretation of External Albanides Structural Model: First Congress of the Balkan Geophysical Society, Athens, Greece.

Gutenberg, B. & Richter, C.F., 1956 Earthquake magnitude, intensity, energy and acceleration. *Bull. seism. Soc. Am.,* **46,** 105–145.

Havskov, J. & Ottemoller, L., 1999. SeisAn Earthquake analysis software, *Seismol. Res. Lett.,* **70,** 532–534.

Havskov, J., Voss, P.H. & Ottemoller, L., 2020. Seismological Observatory Software: 30 Yr of SEISAN. *Seismol. Res. Lett.,* **91**(3), 1846–1852.

Hirose, H., Hirakara, K., Kimata, F., Fujii, N. & Miyazaki, S., 1999. Aslow thrust slip event following the two 1996 Hyuganada earthquakesbeneath the Bungo Channel, southwest Japan, *Geophys. Res. Lett.,* **26,** 3237–3240.

IGEO catalog, https://www.geo.edu.al.

Jolivet, R., Grandin, R., Lasserre, C., Doin, M.P. & Peltzer, G., 2011. Systematic InSAR tropospheric phase delay corrections from global meteorological reanalysis data, *Geophys. Res. Lett.,* **38**(17), doi:10.1029/2011GL048757.

Jouanne, F. *et al.*, 2012. GPS constraints on current tectonics of Albania, *Tectonophysics,* **554-557,** 50–62.

Kostoglodov, V., Singh, S.K., Santiago, J.A., Franco, S.I., Larson, K.M., Lowry, A.R. & Bilham, R., 2003. A large silent earthquake in the Guerrero seismic gap, Mexico, *Geophys. Res. Lett.,* **30,** 1807.

Kuk, V., Prelogovíc, E. & Dragîcevíc, I., 2000. Seismotectonically active zones in the Dinarides, *Geologica Croatica,* **53,** 295–303.

Larson, K.M., Kostoglodov, V., Lowry, A., Hutton, W., Sanchez, O., Hudnut, K. & Suárez, G., 2004. Crustal deformation measurements in Guerrero, Mexico, *J. geophys. Res.,* **109**(4), doi:10.1029/2003JB002843.

Lekkas, E., Mavroulis, S., Papa, D. & Carydis, P., 2019. The 26 November, 2019 Mw 6.4 Durrës (Albania) earthquake.

Li, S., Wdowinski, S., Hsu, Y.-J. & Shyu, J.B.H., 2020. Earthquake interactions in central Taiwan: probing Coulomb stress effects due to ML≥ 5.5 earthquakes from 1900 to 2017, *J. geophys. Res.,* **125,** e2019JB019010.

Lowry, A., 2006. Resonant slow fault slip in subduction zones forced by climatic load stress, *Nature,* **442,** 802–805.

Lowry, A.R., Larson, K.M., Kostoglodov, V. & Bilham, R., 2001. Transient fault slip in Guerrero, southern Mexico, *Geophys. Res. Lett.,* **28,** 3753–3756.

Mavroulis, S., Lekkas, E. & Carydis, P.. 2021. Liquefaction phenomena induced by the 26 November 2019 Mw = 6.4 Durrës (Albania) earthquake and liquefaction susceptibility assessment in the affected area, *Geosciences,* **11**(5), doi:10.3390/geosciences11050215.

Medvedev S. Sponheuer, W. & Karník, V., 1964. Neue seismische Skala Intensity scale of earthquakes, 7. Tagung der Europäischen Seismologischen Kommission vom 24.9. bis 30.9.1962, in *Institut für Bodendynamik und Erdbebenforschung in Jena,* Vol. **77,** pp. 69–76, ed. Jena, V., Deutsche Akademie der Wissenschaften zu Berlin [MSK-64].

Mëhillka, L., Canaj, B. & Banaj, M., 1996. The role of transversal tectonic faults in tectonic style, structural model and geodynamical evolution of the Ionian zone, in *Proceedings of the 1st Congress of the Balkan Geophysical Society,* Athens, Greece, September 2–27.

Mëhillka, L., Dore, P. & Gjika, A., 1999. New structural styles and independent petroleum systems in Outer Albanides, in *Proceedings of the 2nd Congress of the Balkan Geophysical Society,* Istanbul, July 5-9, 1999.

Métois, M., *et al.*, 2020. Subsidence associated with oil extraction, measured from time series analysis of Sentinel-1 data: case study of the Patos-Marinza oil field, Albania, *Solid Earth,* **11**(2), 363–378.

Mignan, A. & Woessner, J., 2012. Estimating the magnitude of completeness for earthquake catalogs. Community Online Resource for Statistical Seismicity Analysis, doi:10.5078/corssa-00180805.

Miller, M.M., Melbourne, T., Johnson, D.J. & Sumner, W.Q., 2002. Periodic slow earthquakes from the Cascadia subduction zone, *Science,* **295,** 2423.

Moshou, A. *et al.*, 2019. A Preliminary Report On The 26 November 2019, Mw = 6.4 DurrëS, Albania. EMSC report published 17 December 2019.

Murekezi, D., Newman, A., Feng, L. & Chen, T., 2020. avnewman/GTDef: GTDef V4 (v4.0.0). Zenodo. doi:10.5281/zenodo.4323169.

Nishani, P., 1985. The analyse of the results of geophysical prospecting for the best knowledge of the geology of the central part of the tectonic zone Kruja and their neighbor zone (In Albanian), *MSc thesis*, Polytechnic University of Tirana.

Ohta, Y., Freymueller, J., Hreinsdóttir, S. & Suito, H., 2006. A large slowslip event and the depth of the seismogenic zone in the south centralAlaska subduction zone, *Earth planet. Sci. Lett.,* **247,** 108–116.

Ohzono, M., Takahashi, H. & Ichiyanagi, M., 2014. An intraplate slow earthquake observed by a dense GPS network in Hokkaido, northernmost Japan, *Geophys. J. Int.,* **200**(1), 144–148.

Ostini, L. 2012. Analysis and quality assessment of GNSS–derived paramter time series, *PhD thesis*, Astronomical Institute, University of Bern, Bern, Switzerland.

Ostini, L., Dach, R., Meindl, M., Schaer, S. & Hugentobler, U. 2008.FODITS: a new tool of the Bernese GPS Software, in *Subcommission for the European Reference Frame (EUREF),* eds Torres, J.A. & Hornik, H.

Ostini, L., Dach, R., Schaer, S., Hugentobler, U., Meindl, M. & Beutler, G.. 2010. Time series analysis using FODITS, in *COST ES0701 WG 1-3 meeting,* Nottingham, UK, Mar. URLU:\Groups\gps\PosterNottiingham2010\PosterNottingham2010Ati. Poster.

Ozawa, S., Murakami, M., Kaidzu, M., Tada, T., Sagiya, T., Hatanaka, Y., Yarai, H. & Nishimura, T., 2002. Detection and monitoring of ongoing aseismic slip in the Tokai region, Central Japan, *Science,* **298,** 1009–1012.

Papa, A. & Kondo, A., 1968. Reflection about the Sazani zone and its transition into Ionian zone (In Albanian, abstract in French): bull. of Tirana University. *Nat. Sci. Ser.,* **2,** 47–55.

Papadopoulos, G.A. *et al.*, 2020. The 26 November 2019 Mw 6.4 Albania destructive earthquake. *Seismol. Res. Lett.,***91,** 3129–3138.

Perfettini, H. & Avouac, J.-P., 2004. Postseismic relaxation driven by brittle creep: A possible mechanism to reconcile geodetic measurements and the decay rate of aftershocks, application to the Chi-Chi earthquake, Taiwan, *J. Geophys. Res.,* **109,** B02304, doi:10.1029/2003JB002488.

Pondrelli, S., Salimbeni, S., Ekstrom, äG., Morelli, A., Gasperini, P. & Vannucci, G., 2006. The Italian CMT dataset from 1977 to the present, *Phys. Earth planet. Inter.,* **159,** 286–303.

Protti, M. *et al.*, 2004. A creep event on the shal-low interface of the Nicoya Peninsula, Costa Rica seismogenic zone, *EOS, Trans. Am. geophys. Un.,* **85,** Fall Meet. Suppl., Abstract S41D-07.

Radiguet, M., Cotton, F., Vergnolle, M., Campillo, M., Valette, B., Kostoglodov, V. & Cotte, N., 2011. Spatial and temporal evolution of a long term slow slip event: the 2006 Guerrero Slow Slip Event. *Geophys. J. Int.,* **184,** 816–828.

Rogers, G. & Dragert, H., 2003. Episodic tremor and slip on the Cascadia subduction zone: the chatter of silent slip. *Science,* **300,** 1942–1943.

Roure, F., Nazaj, S., Mushka, K., Fili, I., Cadet, J.P. & Bonneau, M., 2004. Kinematic evolution and petroleum systems: an appraisal of the Outer Albanides, in *Thrust Tectonics and Hydrocarbon Systems,* pp. 474–493, ed. McClay, *AAPG Mem*., **82**.

Rovida, A. & Antonucci, A., 2021. EPICA - European PreInstrumental Earthquake Catalogue, version 1.1. Istituto Nazionale di Geofisica e Vulcanologia (INGV).

Schmitz, B., Biermanns, P., Hinsch, R., Đaković, M., Onuzi, K., Reicherter, K. & Ustaszewski, K., 2020. Ongoing shortening in the Dinarides fold-and-thrust belt: a new structural model of the 1979 (Mw 7.1) Montenegro earthquake epicentral region, *J. Struct. Geol.,* **141,** 104192.

Seitaj, H., Mëhillka, L., Xhelili, A. & Kamberi, Th., 1996. Complex interpretation of seismic and geological data of Western orogenic front of Ionian zone and prospect of this area, in *Poceedings of the 1st Congress of the Balkan Geophysical Society,* Athens, September 23–27.

Storchak, D.A., Di Giacomo, D., Engdahl, E.R., Harris, J., Bondár, I., Lee, W.H.K., Bormann, P. & Villaseñor, A., 2015. The ISC-GEM Global Instrumental Earthquake Catalogue (1900-2009): introduction, *Phys. Earth planet. Inter.,* **239,** 48–63.

Stucchi, M. *et al.*, 2012. The SHARE European Earthquake Catalogue (SHEEC) 1000-1899, *J. Seismol.,* **17,** 523–544.

Sulstarova, E., 1983.The focal mechanism of the April 15, 1979 earthquake sequence, in Bisztricsany, É & Szeidovitz, G.Y., eds, *Developments in Solid Earth Geophysics : European Seismological Commission,* Elsevier, pp. 161–165.

Sulstarova, E., 1996. Earthquake hazard assessment in Albania, in *Risque, nature et société: Actes du séminaire ≪ Delphes I ≫ [online],* pp. 199-216, Paris: Éditions de la Sorbonne, 1996 (generated 16 mars 2023). Available on the Internet. ISBN: 9791035101275. https://doi.org/10.4000/books.psorbonne.32094.

Sulstarova, E. & Koçiaj, S., 1975. "The Catalogue of Albanian Earthquakes", *Publication of Seismological Centre of Academy of Sciences (in Albanian),* Tirana, 225p.

Sulstarova, E., Muço, B., Koçiaj, S. & Peçi, V., 2003. *Catalogue of Earthquakes of Albania Ms ≥ 4.5, period 58BC-2000 (Katalogu i termeteve te Shqiperise, periudha 58-2000, Ms ≥4.5),,* Archive of the Institute of Seismology.

Szeliga, W., Melbourne, T.I., Miller, M.M. & Santillan, V.M., 2004. Southern Cascadia episodic slow earthquakes, *Geophys. Res. Lett.,* **31**(16), doi:10.1029/2004GL020824.

Teloni, S., Invernizzi, C., Mazzoli, S., Pierantoni, P. & Spina, V., 2020. The seismogenic fault system of the M_w 6.4, November 2019 Albania earthquake: new insights into the structural architecture and active tectonic setting of the outer Albanides, *J. Geol. Soc.,* **178**(2), doi:10.1144/jgs2020-193.

Thatcher, W., 2001. Silent slip on the Cascadia subduction interface, *Science,* **292,** 1495–1496.

Valbona, U. & Misha, V., 1987. Some problems on the determination of the margin between their belts and chains based on surface surveys and other data of the complex, (In Albanian, abstract in English), *Bull. Oil Gas,* **1,** 3–14.

Valkaniotis, S. *et al.*, 2020. The Mw = 5.6 Kanallaki Earthquake of 21 March 2020 in West Epirus, Greece: reverse Fault Model from InSAR Data and seismotectonic implications for Apulia-Eurasia collision, *Geosciences,* **10,** 454, doi:10.3390/geosciences10110454.

Velaj, T., 1999. The effect of the evaporite tectonic in the structural model of the Berati belt of Albanides, in *Proceedings of the 2nd Congress of the Balkan Geophysical Society,* Istanbul, Turkey, July 5–9.

Velaj, T., 2001. Evaporites in Albania and their impact on the thrusting processes. *J. Balkan Geophys. Soc.,* **4,** 9–18.

Vergnolle, M., Walpersdorf, A., Kostoglodov, V., Tregoning, P., Santiago, J.A., Cotte, N. & Franco, S.I., 2010. Slow slip events in Mexico revised from the processing of 11 year GPS observations, *J. geophys. Res.,* **115**(B8), doi:10.1029/2009JB006852.

Waldhauser, F., 2001. HypoDD: a computer program to compute double-difference earthquake locations, USGS Open File Rep., 01-113, 2001.

Waldhauser, F. & Ellsworth, W.L., 2000. A double-difference earthquake location algorithm: method and application to the Northern Hayward Fault, California. *Bull. seism. Soc. Am.,* **90**(6), 1353–1368.

Wallace, L.M., Kaneko, Y., Hreinsdóttir, S., Hamling, I., Peng, Z., Bartlow, N., D'Anastasio, E. & Fry, B., 2017. Large-scale dynamic triggering of shallow slow slip enhanced by overlying sedimentary wedge. *Nat. Geosci.,* **10,** 765–770.

Wang, L., Wang, R., Roth, F., Enescu, B., Hainzl, S. & Ergintav, S., 2009. Afterslip and viscoelastic relaxation following the 1999 M 7.4 Izmit earthquake from GPS measurements, *Geophys. J. Int.,* **178,** 1220–1237.

Wang, R., Parolai, S., Ge, M., Jin, M., Walter, T.R. & Zschau, J., 2012. The 2011 Mw 9.0 Tohoku Earthquake: comparison of GPS and strong-motion data, *Bull. seism. Soc. Am.,* **103**(2B), 1336–1347.

Wang, R., Schurr, B., Milkereit, C., Shao, Zh. & Jin, M., 2011. An improved automatic scheme for empirical baseline correction of digital strong-motion records, *Bull. seism. Soc. Am.,* **101,** 2029–2044.

Xhufi, C. & Canaj, B., 1999. Some aspects of seismic-geologic interpretation in thrusting belts, in *Proceedings of the 2nd Congress of the Balkan Geophysical Society,* Istanbul, Turkey, July 5–9.

SUPPORTING INFORMATION

Supplementary data are available at *GJI* online.

Appendix_A.docx

Appendix_B.docx
Appendix_C.docx

Please note: Oxford University Press is not responsible for the content or functionality of any supporting materials supplied by the authors. Any queries (other than missing material) should be directed to the corresponding author for the paper.

APPENDIX A: INSTRUMENTAL SEISMICITY

A.1 ALBANIA SEISMIC NETWORK

The Albania Seismic network is composed of six seismic stations: TIR, PHP, SDA, BBA1, VLO and KBN. The nearest station to the earthquake epicentre is the Tirana station (TIR), 33 km east of Durrës, causing an erroneous location and undefined seismic depth. The Tirana (TIR) station is equipped with an STS-2 (VBB) sensor. The Peshkopia (PHP) broadband (BB) seismic station, located more than 100 km to the NE of the epicentre area, it operates at a frequency band of 0.033–50 Hz. The Shkodra (SDA) station, located around 60 km NNW of the epicentre area, is settled on limestones and equipped with a broadband (BB) Guralp-40T (40 sec) sensor, and it operates in the same frequency range as the PHP station. Over 100 km away from the epicentral area, three more stations could detect and record the earthquake: the Vlora (VLO) station located S, the Korca (KBN) seismic station located SE, and the BBA1 deployed into Marinza oilfield (Métois *et al.* 2020) in a borehole operation way aiming detection of exploitation related triggered micro-earthquakes (Fig. A1). A number of regional seismic stations port of European Agencies like Italian National seismic Network operated by the National Institute of Geophysics and volcanology (INGV) and Aristotle university Seismic Network (AUTH) are permanently exchanging data with ASN, to increase the regional capability of detection and earthquake location accuracy.

A.2 INSTRUMENTAL SEISMICITY IN DURRES AREA

The active area of Durres has been characterized by an intense seismic activity after the main shock based on instrumental catalogues covering the area ISC (https://www.isc.ac.uk/Bull) and IGEO (https://geo.edu.al). If we focus on the main shock and the corresponding aftershocks $M_L \geq 2.8$, for the time span between April 2018 to April 2021, a number of 188 seismic events could be clearly evidenced (see Figs 3a and b; Table A1). The main characteristics of this polygon is the seismogenic depth largely varying between 0 and 50 km, predominantly concentrating at 20 km of depth, as the most probable. Data are listed in Table A1 and displayed in the Fig. 3(a). The relocation is realized with HypoDD software (Waldhauser & Ellsworth 2000; Waldhauser 2001) implemented in SEISAN—Earthquake Analysis Software (Havskov & Ottemoller 1999; Havskov *et al.*2020).

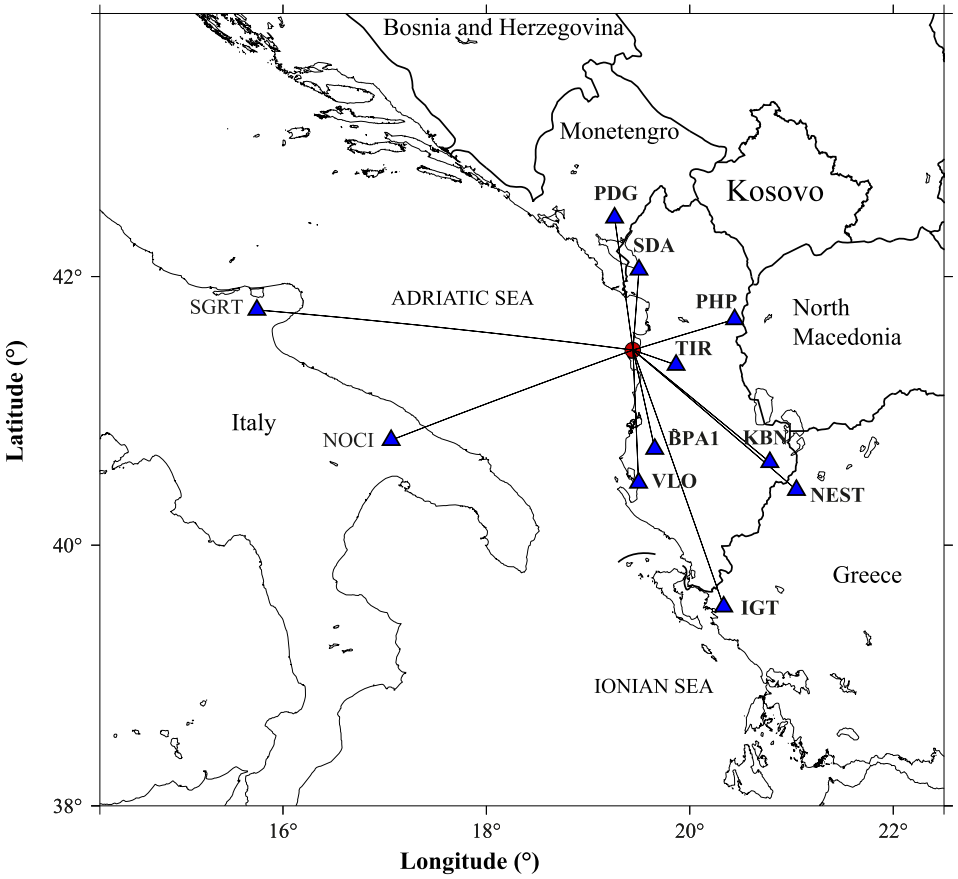

Figure A1. The locations of the stations that detected the 26 November 2019 earthquake belong to ASN, INGV, AUTH and Podgorica in Montenegro (blue triangles).

Table A1. The seismic activity in Durrës area for the time span 2018–2021 and magnitude range $M_L \geq 2.8$.

No.	Date dd/mm/yyyy	Origin Time hh:mm	Latitude NS	Longitude EW	Depth (km)	M_w
1	27/04/2018	05:51	41.546	19.51	32.8	3
2	04/07/2018	09:01	41.465	19.495	18.3	4.9
3	04/07/2018	09:08	41.484	19.483	22.1	4.2
4	04/07/2018	09:11	41.551	19.636	31.8	2.9
5	04/07/2018	11:24	41.463	19.467	13.9	4.1
6	04/07/2018	11:30	41.502	19.686	24.8	3.2
7	04/07/2018	11:32	41.525	19.427	24.2	3.3
8	04/07/2018	11:35	41.51	19.516	29.7	3.7
9	04/07/2018	11:42	41.589	19.534	46.1	3.5
10	04/07/2018	12:06	41.505	19.647	26.2	3
11	04/07/2018	13:33	41.466	19.603	18.5	3.8
12	04/07/2018	15:52	41.478	19.599	28.6	2.9
13	04/07/2018	16:36	41.451	19.544	28.9	3.8
14	04/07/2018	04:08	41.513	19.469	14.5	3.3
15	05/07/2018	02:09	41.567	19.49	41.7	3.8
16	05/07/2018	03:17	41.483	19.621	17.9	2.9
17	05/07/2018	04:20	41.461	19.483	6.1	3
18	05/07/2018	11:03	41.494	19.455	24.9	3.4
19	05/07/2018	22:48	41.456	19.474	22.9	4.2
20	05/07/2018	22:51	41.494	19.55	24.6	3.6
21	07/07/2018	07:41	41.516	19.514	31.3	2.9
22	13/07/2018	08:23	41.49	19.499	29.2	2.9

Table A1. Continued

No.	Date dd/mm/yyyy	Origin Time hh:mm	Latitude NS	Longitude EW	Depth (km)	M_w
23	14/07/2018	17:30	41.488	19.453	32.8	2.9
24	15/07/2018	10:21	41.522	19.452	49.7	3.6
25	09/08/2018	02:37	41.553	19.456	46	3.5
26	18/09/2018	19:04	41.486	19.515	27	3
27	08/11/2018	20:01	41.472	19.541	25.1	2.8
28	16/02/2019	16:20	41.486	19.736	2	4.5
29	17/02/2019	21:21	41.419	19.406	32	5.8
30	31/03/2019	07:51	41.549	19.389	13.7	3.1
31	31/03/2019	17:59	41.542	19.393	14.9	3
32	31/03/2019	19:09	41.528	19.391	13.3	3.1
33	31/03/2019	20:04	41.575	19.439	11.8	3
34	31/03/2019	20:38	41.491	19.353	25	3.5
35	31/03/2019	22:14	41.494	19.349	24.1	3.7
36	01/04/2019	11:57	41.471	19.317	21	3.1
37	22/04/2019	14:07	41.489	19.486	26.6	3.1
38	23/04/2019	08:58	41.539	19.613	11.8	3.8
39	23/04/2019	16:46	41.501	19.608	25	3.2
40	28/08/2019	11:55	41.202	19.71	38.4	2.9
41	21/09/2019	14:04	41.571	19.493	28.1	5.6
42	21/09/2019	14:15	41.55	19.533	33.6	5.1
43	21/09/2019	16:10	41.438	19.453	44.8	4
44	21/09/2019	16:32	41.506	19.573	32	2.9
45	21/09/2019	21:02	41.371	19.393	42.2	2.9
46	05/10/2019	23:55	41.476	19.428	36.9	3.1
47	30/10/2019	13:13	41.407	19.596	18.5	2.9
48	17/11/2019	23:16	41.463	19.525	5.2	3
49	25/11/2019	20:57	41.451	19.515	17.8	3.5
50	25/11/2019	20:57	41.417	19.487	0	3.7
51	25/11/2019	23:24	41.42	19.513	8.8	2.9
52	26/11/2019	01:47	41.404	19.491	16.8	4.5
53	26/11/2019	01:47	41.426	19.478	5.7	4.5
54	26/11/2019	02:19	41.435	19.542	5.2	3.2
55	26/11/2019	02:54	41.411	19.546	13.9	5.9
56	26/11/2019	03:03	41.515	19.738	6.3	4.3
57	26/11/2019	03:04	41.51	19.596	18.6	3.7
58	26/11/2019	03:57	41.596	19.445	14	4
59	26/11/2019	04:09	41.276	19.59	22.8	3.4
60	26/11/2019	04:21	41.497	19.592	14	4.1
61	26/11/2019	04:42	41.547	19.582	14	3.7
62	26/11/2019	04:46	41.488	19.567	0	3.6
63	26/11/2019	05:32	41.482	19.56	6	3.5
64	26/11/2019	05:50	41.556	19.649	10.8	3.9
65	26/11/2019	06:44	41.483	19.611	16	3.7
66	26/11/2019	06:54	41.445	19.589	5.1	3.9
67	26/11/2019	07:12	41.591	19.519	22.3	4.1
68	26/11/2019	07:15	41.588	19.598	7.3	3.1
69	26/11/2019	07:36	41.44	19.551	18.2	4.6
70	26/11/2019	07:40	41.573	19.595	5.3	3.7
71	26/11/2019	09:13	41.508	19.659	5.1	3.5
72	26/11/2019	09:47	41.58	19.667	16	4.1
73	26/11/2019	10:09	41.552	19.584	10.8	4
74	26/11/2019	11:52	41.551	19.626	0	3.1
75	26/11/2019	12:14	41.464	19.595	5.1	4
76	26/11/2019	12:46	41.559	19.599	5.1	3.4
77	26/11/2019	15:03	41.466	19.624	19.5	2.9
78	26/11/2019	15:11	41.575	19.53	12	3.6
79	26/11/2019	15:16	41.488	19.602	15	3.9
80	26/11/2019	15:59	41.455	19.674	5.2	3.9
81	26/11/2019	16:27	41.513	19.485	6	2.9
82	26/11/2019	16:34	41.513	19.632	5.1	4
83	26/11/2019	17:06	41.533	19.645	16	4.1
84	26/11/2019	17:09	41.589	19.678	16	4
85	26/11/2019	18:50	41.428	19.568	6	2.9
86	26/11/2019	18:54	41.486	19.723	6	3.1

Table A1. Continued

No.	Date dd/mm/yyyy	Origin Time hh:mm	Latitude NS	Longitude EW	Depth (km)	M_w
87	26/11/2019	19:06	41.567	19.577	16	3
88	26/11/2019	19:44	41.553	19.606	6	3.7
89	26/11/2019	22:46	41.521	19.516	6	3.7
90	26/11/2019	23:20	41.541	19.568	5.2	3.4
91	27/11/2019	00:06	41.553	19.48	6	3.2
92	27/11/2019	00:41	41.572	19.426	6	3.4
93	27/11/2019	02:08	41.554	19.577	6	3
94	27/11/2019	03:52	41.594	19.548	5.3	3.7
95	27/11/2019	05:11	41.589	19.505	6	3.4
96	27/11/2019	05:39	41.566	19.524	10.6	3.3
97	27/11/2019	06:10	41.58	19.508	6	3.5
98	27/11/2019	06:45	41.533	19.609	15	3
99	27/11/2019	07:13	41.537	19.562	0	3.3
100	27/11/2019	08:11	41.501	19.654	11.8	2.9
101	27/11/2019	10:55	41.552	19.516	10	3
102	27/11/2019	10:59	41.548	19.565	4.2	3.1
103	27/11/2019	11:03	41.543	19.585	10	4.2
104	27/11/2019	12:02	41.576	19.49	16	3.2
105	27/11/2019	12:47	41.417	19.49	5.3	3.3
106	30/11/2019	01:24	41.534	19.588	5.8	3.1
107	30/11/2019	04:28	41.582	19.527	6	3.1
108	30/11/2019	05:05	41.517	19.468	12	3
109	30/11/2019	05:16	41.54	19.564	5.1	3.5
110	30/11/2019	20:53	41.545	19.577	6	4.6
111	30/11/2019	22:54	41.59	19.53	0.4	3.3
112	01/12/2019	06:04	41.574	19.573	25.3	4
113	01/12/2019	06:52	41.584	19.451	2	3.2
114	01/12/2019	07:18	41.561	19.511	37.3	3.6
115	01/12/2019	11:42	41.341	19.464	27.9	3.8
116	01/12/2019	17:48	41.549	19.631	41.9	3.6
117	02/12/2019	22:41	41.532	19.725	38.7	3.4
118	02/12/2019	08:26	41.488	19.697	34	4.2
119	02/12/2019	16:43	41.446	19.678	10.4	3.6
120	02/12/2019	23:23	41.543	19.733	35.5	3.9
121	03/12/2019	12:50	41.539	19.561	25	2.9
122	04/12/2019	01:08	41.492	19.613	9.4	2.9
123	04/12/2019	02:33	41.542	19.494	33.2	3.1
124	04/12/2019	07:47	41.498	19.613	12.1	3
125	04/12/2019	10:06	41.387	19.695	25.9	2.9
126	05/12/2019	03:04	41.578	19.538	32.1	3
127	06/12/2019	04:28	41.584	19.648	27.9	3.3
128	06/12/2019	23:18	41.539	19.352	24.8	3.5
129	07/12/2019	16:51	41.585	19.637	30.5	3
130	07/12/2019	18:16	41.507	19.642	3.7	3
131	09/12/2019	05:29	41.567	19.499	31	3.8
132	09/12/2019	14:53	41.568	19.487	18.1	3.4
133	09/12/2019	14:58	41.514	19.469	32	3.4
134	09/12/2019	18:10	41.534	19.612	32.5	3.1
135	10/12/2019	09:00	41.525	19.544	27.4	3.3
136	11/12/2019	00:30	41.539	19.331	35.2	3.5
137	13/12/2019	03:10	41.448	19.427	38.2	3
138	14/12/2019	22:25	41.543	19.46	35.8	3
139	15/12/2019	01:18	41.495	19.559	46.2	3.9
140	19/12/2019	16:03	41.392	19.466	28.9	4.2
141	26/12/2019	06:17	41.516	19.501	46.1	2.9
142	30/12/2019	18:34	41.563	19.586	15.4	3
143	02/01/2020	02:02	41.591	19.372	7.6	2.9
144	03/01/2020	16:37	41.548	19.396	9.2	3
145	08/01/2020	06:01	41.535	19.444	7.2	2.9
146	12/01/2020	23:25	41.519	19.557	31.7	2.9
147	27/01/2020	01:40	41.479	19.679	33.5	3.5
148	28/01/2020	20:15	41.496	19.646	7.1	4.7
149	28/01/2020	20:17	41.503	19.724	13.5	4.1
150	28/01/2020	20:31	41.537	19.628	33.3	3

Table A1. Continued

No.	Date dd/mm/yyyy	Origin Time hh:mm	Latitude NS	Longitude EW	Depth (km)	M_w
151	31/01/2020	21:05	41.541	19.53	36.4	3.9
152	13/02/2020	19:10	41.444	19.664	36.4	3.3
153	26/02/2020	19:52	41.485	19.517	37.1	3
154	27/02/2020	14:31	41.428	19.586	36.8	3
155	02/03/2020	09:23	41.474	19.531	28.9	3
156	19/03/2020	09:20	41.597	19.475	2	3.6
157	19/03/2020	13:25	41.577	19.323	24.6	3
158	20/03/2020	07:06	41.434	19.381	5.6	2.9
159	29/03/2020	13:37	41.565	19.457	28.1	2.9
160	12/04/2020	22:03	41.543	19.466	82.2	3
161	13/04/2020	16:43	41.55	19.309	38.8	3.4
162	16/04/2020	17:27	41.162	19.74	38.3	3.1
163	20/04/2020	20:13	41.46	19.364	12.6	2.9
164	22/04/2020	22:08	41.314	19.616	49	3
165	27/04/2020	20:15	41.51	19.71	34	3.3
166	01/06/2020	20:21	41.539	19.569	46.5	3.3
167	07/06/2020	23:52	41.529	19.611	23.2	3.6
168	08/06/2020	15:21	41.488	19.582	5.9	4.1
169	25/06/2020	07:53	41.464	19.585	32	3.3
170	19/07/2020	04:56	41.5	19.478	23.3	3.1
171	23/07/2020	17:23	41.541	19.446	28.2	3.5
172	22/08/2020	10:25	41.554	19.645	35.4	3.4
173	10/09/2020	05:00	41.54	19.413	2.1	3.4
174	18/09/2020	20:30	41.486	19.702	17.2	3
175	23/09/2020	05:30	41.421	19.532	11.2	3.5
176	07/10/2020	22:13	41.501	19.358	2	3.9
177	07/10/2020	22:25	41.499	19.485	23.8	3
178	07/10/2020	23:44	41.543	19.427	25.2	3.4
179	09/10/2020	14:36	41.596	19.575	35.4	3.8
180	06/12/2020	07:19	41.558	19.594	11.6	4
181	26/12/2020	18:04	41.466	19.561	2	3.3
182	12/01/2021	13:49	41.306	19.75	184.3	3
183	24/01/2021	08:30	41.507	19.526	26.3	3.2
184	24/01/2021	17:35	41.387	19.65	108.7	3.6
185	26/01/2021	14:32	41.591	19.505	18.5	3.9
186	24/02/2021	03:07	41.558	19.706	30.7	3.1
187	05/04/2021	04:39	41.454	19.608	20.1	3.1
188	07/04/2021	02:06	41.537	19.525	7.7	3.3

APPENDIX B: DATA AND TIME-SERIES

B.1 COSEISMIC SLIP ESTIMATION

The GNSS measurements performed before and after the earthquake, both on campaign (see Table 2) and permanent points (see Table 2), allowed the quantification of the coseismic displacements associated with the main shock (see Fig. 4). To calculate coseismic slip for GPS stations, we used nine stations (see Table 3), from which four were measured during campaigns, and six were permanent stations (Fig. B1). For campaign points, extrapolation of time-series until the day of the main shock is performed using interseismic velocities estimated in the IGb14 reference frame. Coseismic slip for campaign measurements was estimated by the difference between the extrapolated position value for the day of the main shock and the position measured after the earthquake.

B.2 THE TIME-SERIES ANALYSIS

We studied the time-series of permanent station recordings after the earthquake. GNSS time-series have been expressed in the IGb14 reference frame (see Figs 5 and B2). Owing to the shutdown of the ALBPOS network just after the main shock, the post-seismic deformation following the main shock is poorly documented, as the ASIG stations taking over from the ALBPOS network did not start their measurements until early 2020. The only station that operated immediately after the main shock was the TIRA station, whereas the KULL station started in mid-December 2019. The time-series do not show a clear post-seismic signal, suggesting that most post-seismic deformation lasted a few weeks. Moreover, the GNSS time-series of stations in Albania showed velocity changes around day + 200, and day + 300 after the main shock around 26 and 28 d, respectively (see Figs 5 and B2). We interpret these velocity changes as the occurrence of transient events interpreted as slow slip events (SSEs).

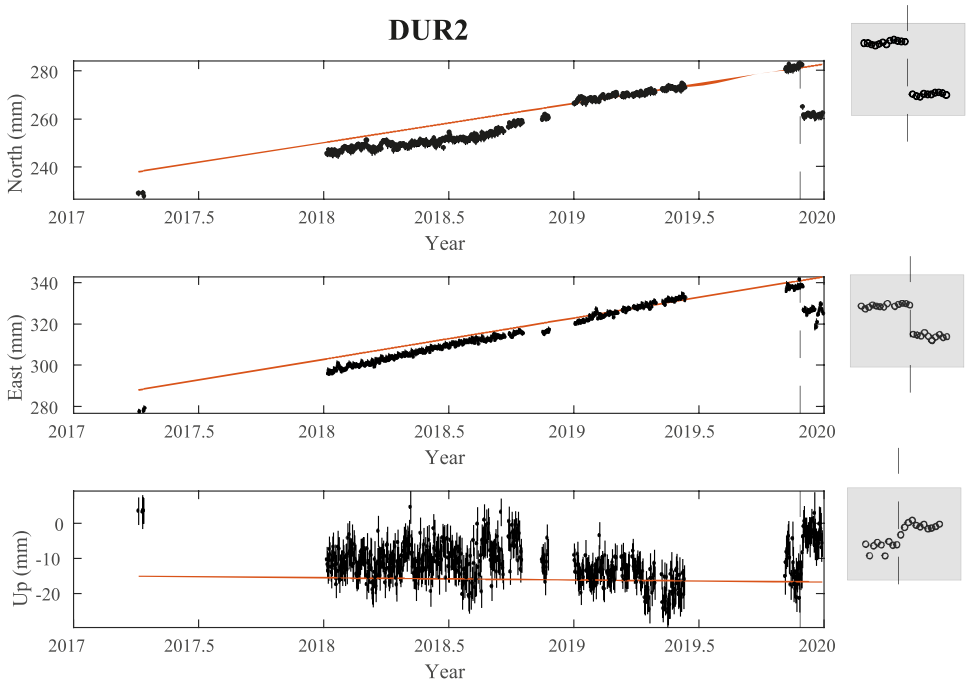

Figure B1. Time-series of the GNSS stations (north, east and up components) of the DUR2, TIR2, TIRA, PESH, SHKO, ORIK and BERA permanent stations and of the GNSS campaign of measurements of 0602, 0608, 0611 and KRYE. The fitting data are represented by the red line.

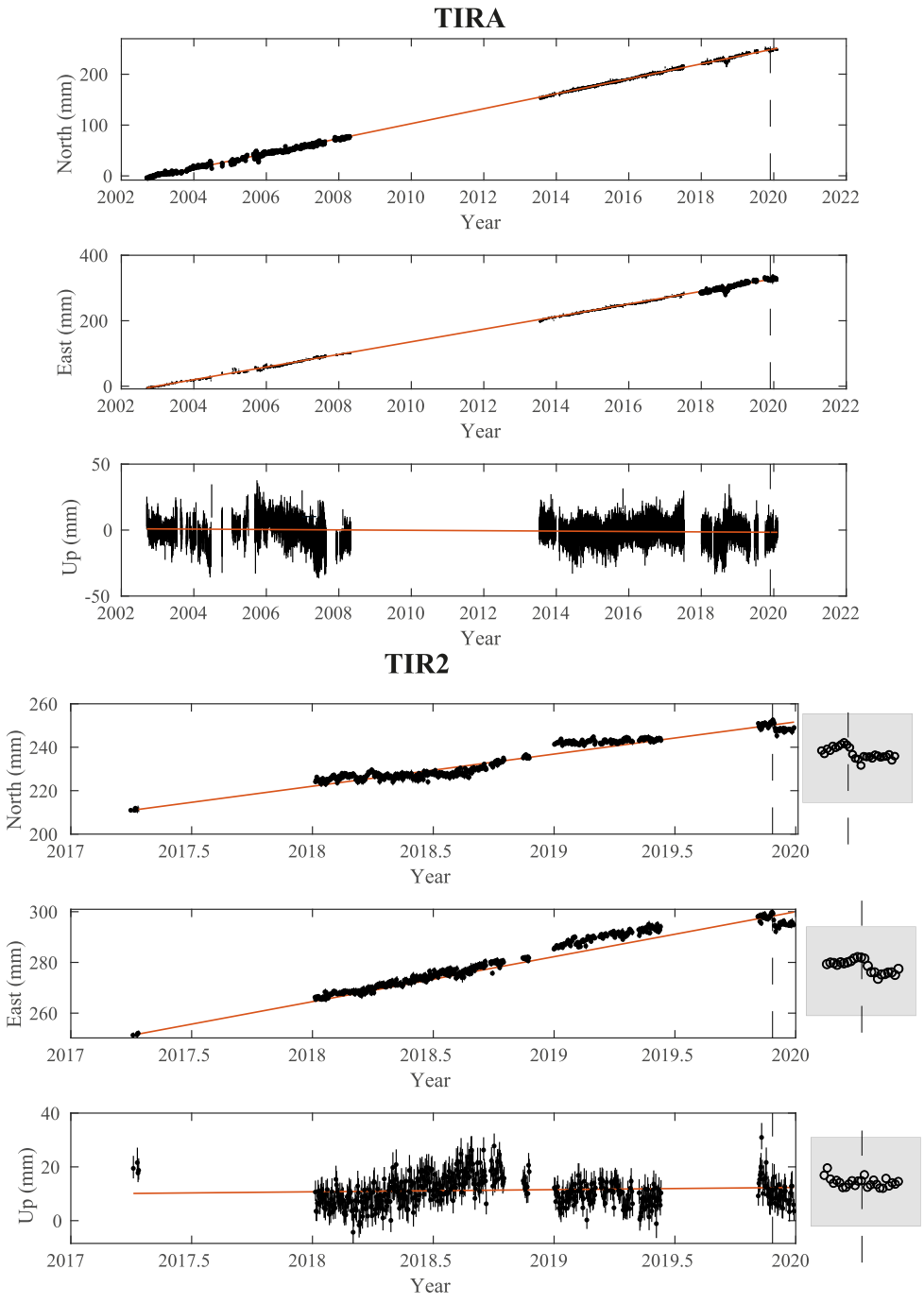

Figure B1. Continued.

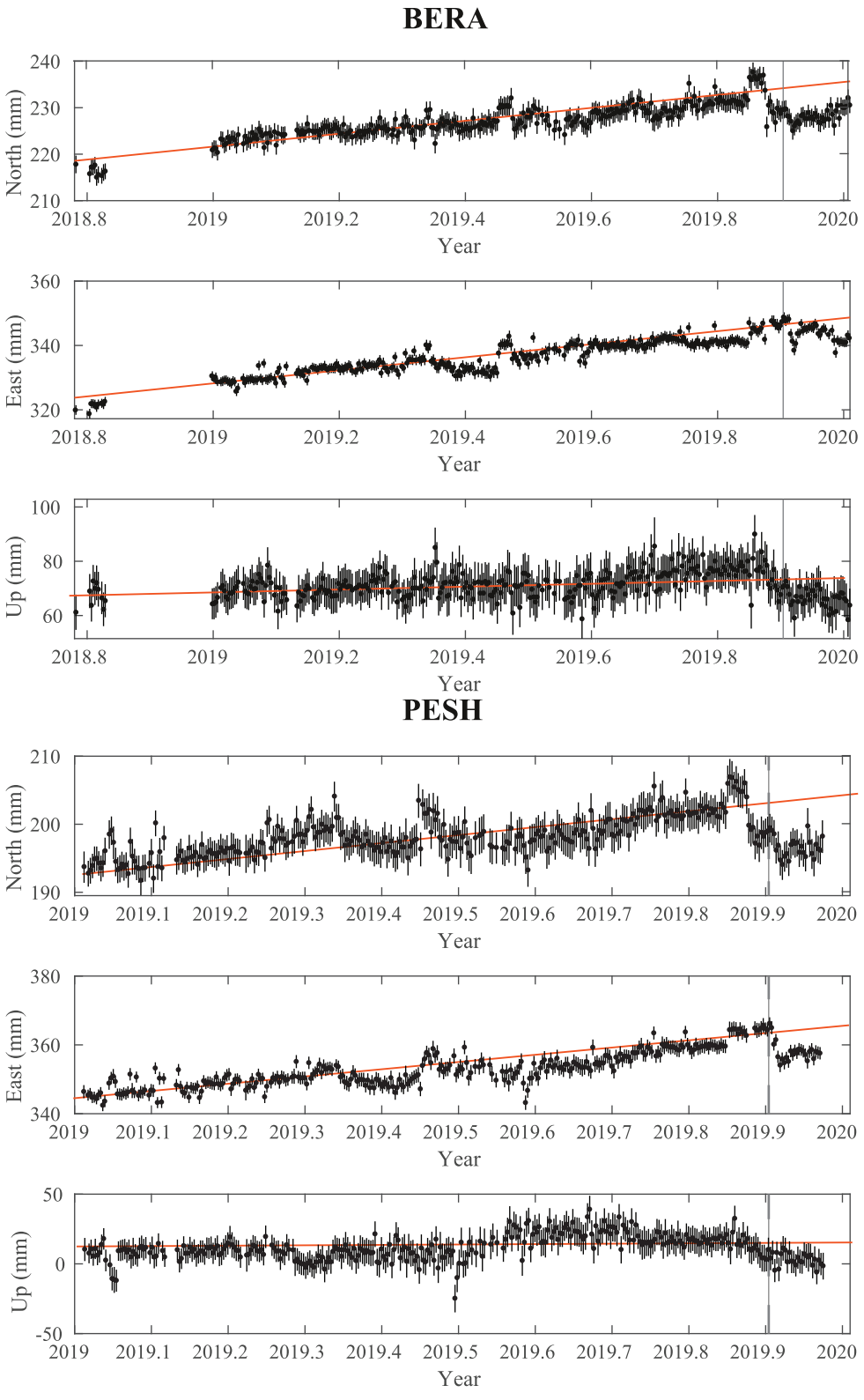

Figure B1. Continued.

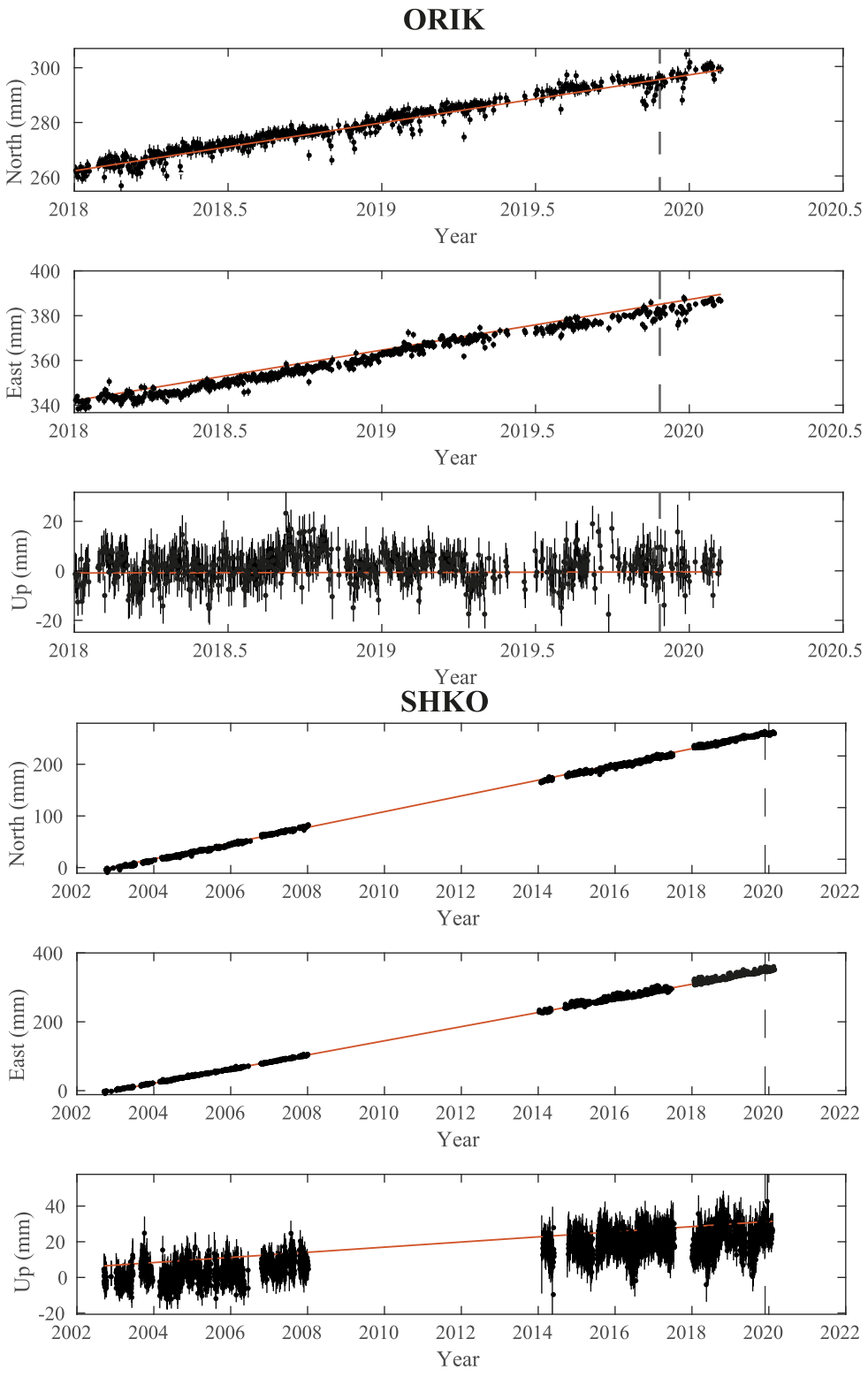

Figure B1. Continued.

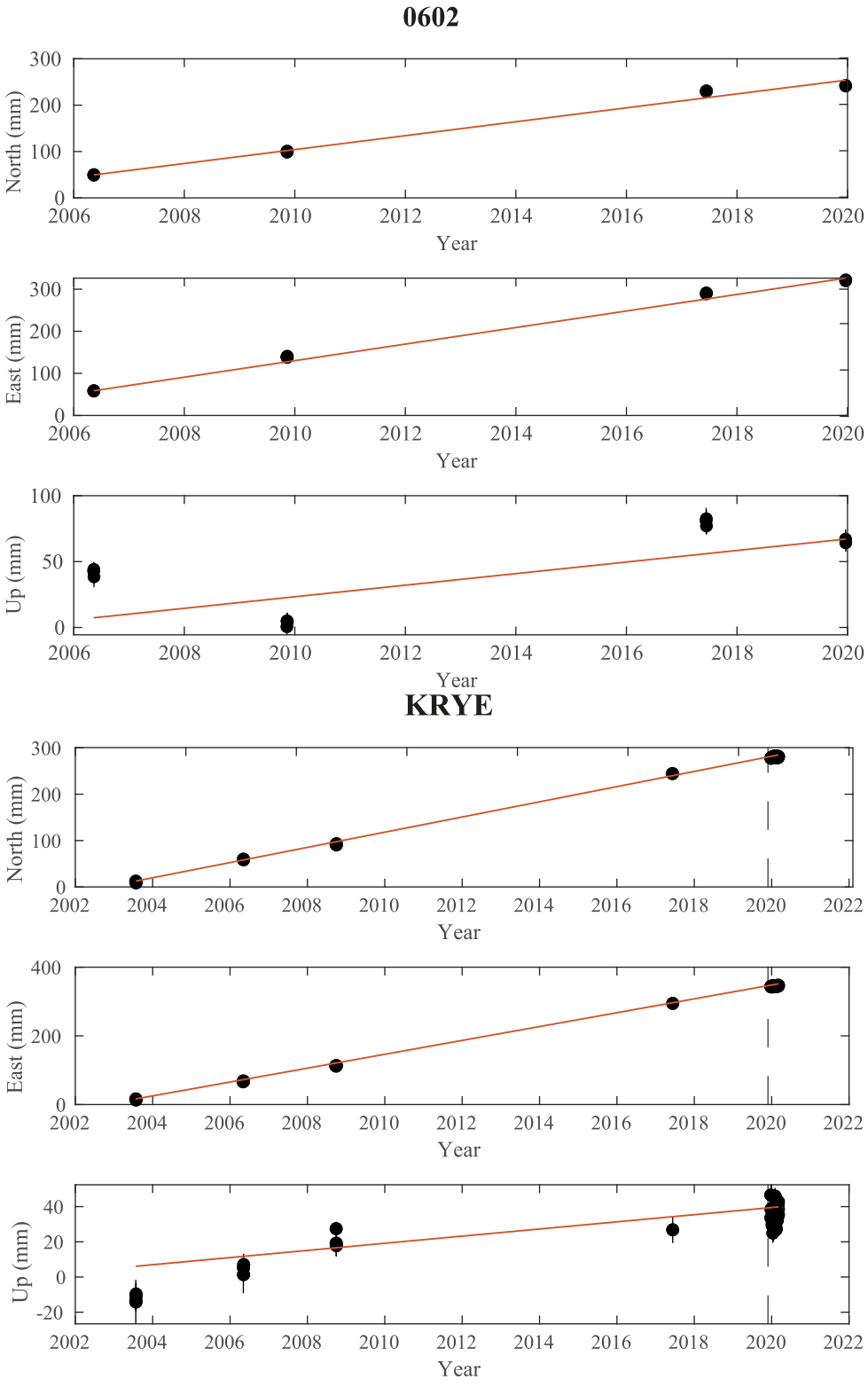

Figure B1. Continued.

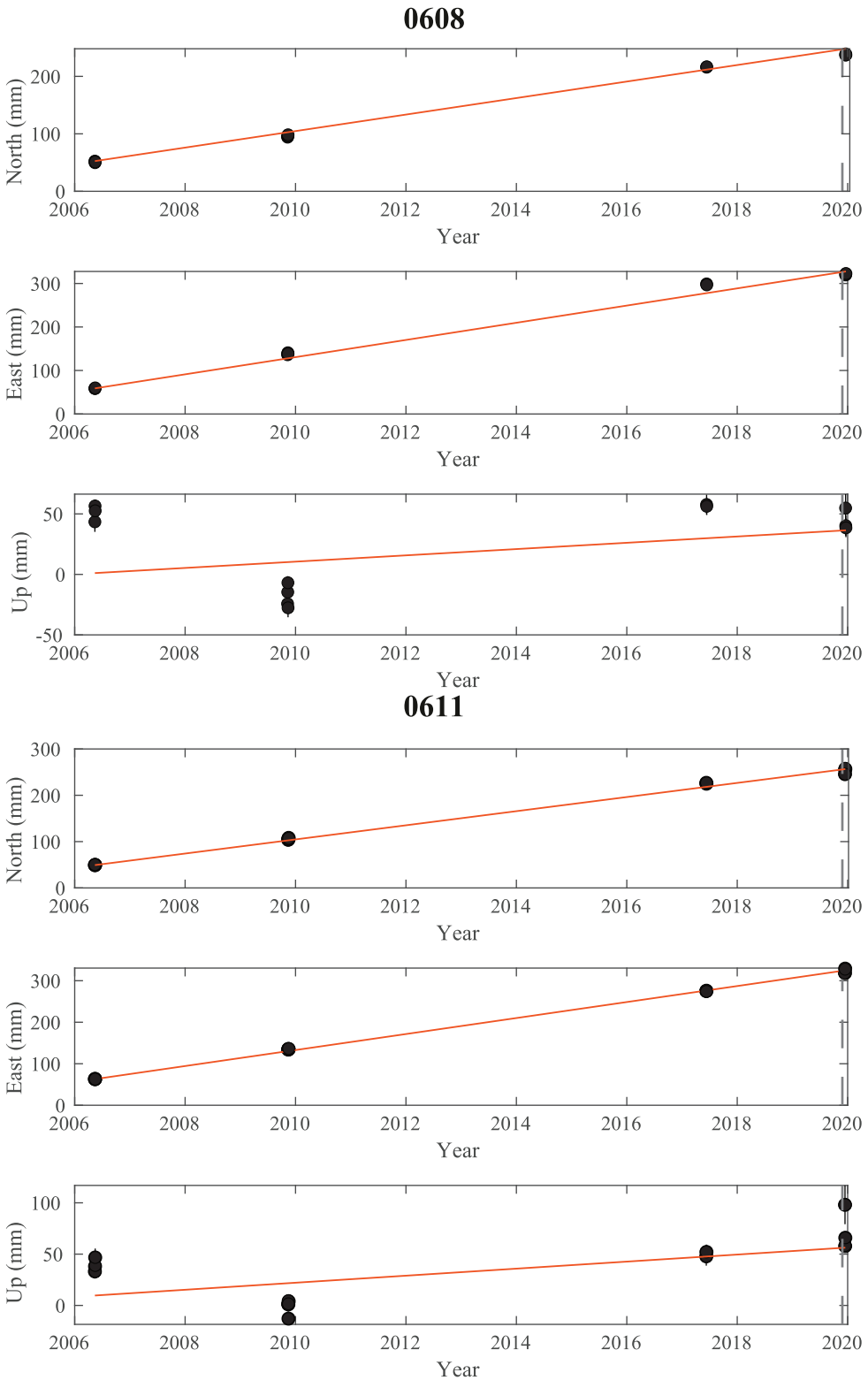

Figure B1. Continued.

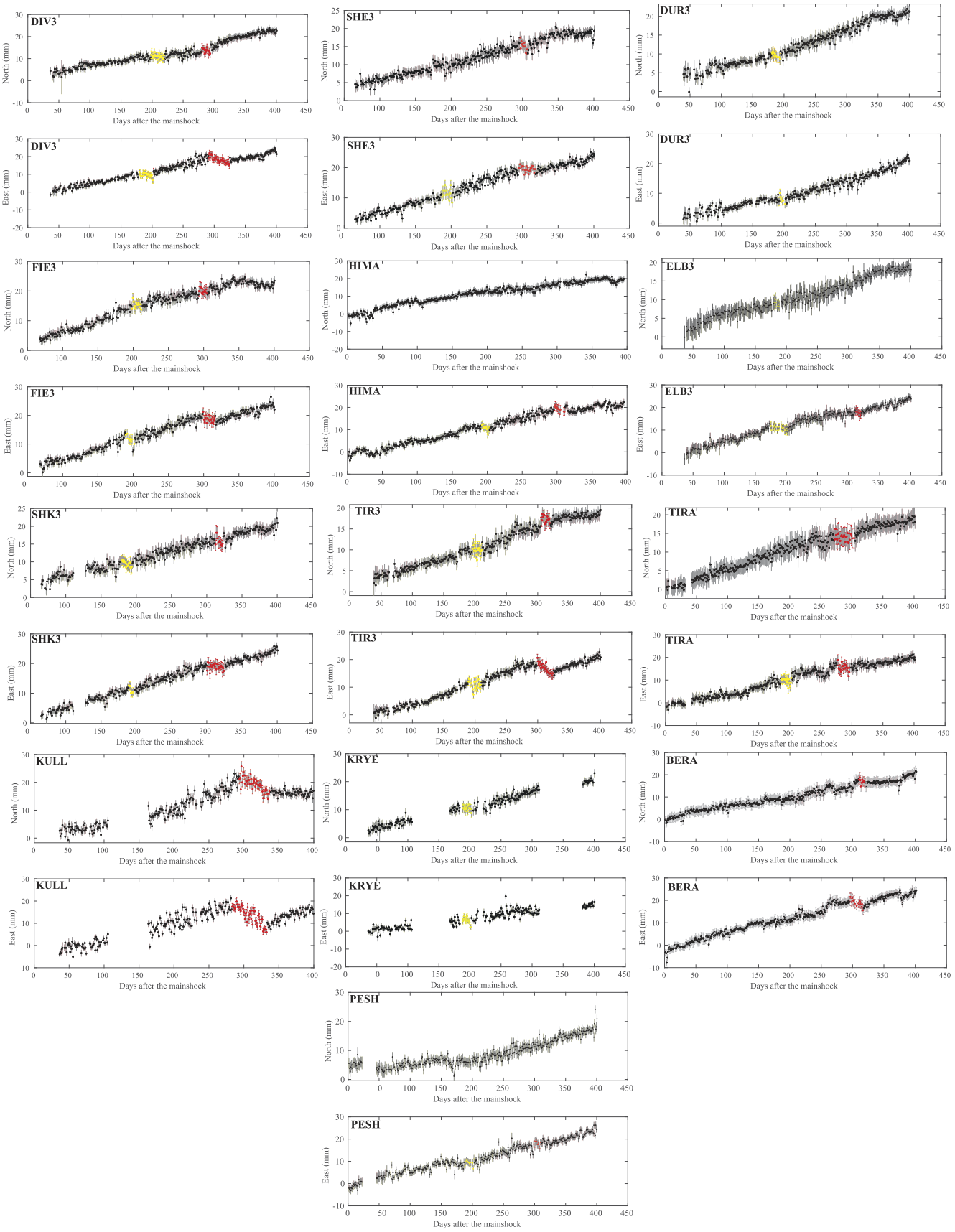

Figure B2. Time-series of the horizontal components (north, east component) measured at the BERA, DUR3, ELB3, DIV3, TIR3, TIRA, KULL, KRYE, DIV3, FIE3, SHE3, SHK3, HIMA, PESH and ELB3 stations. The figures show the trending time evolution of displacement. Occurrence of SSE for s + 200 events (yellow) and + 300 events (red).

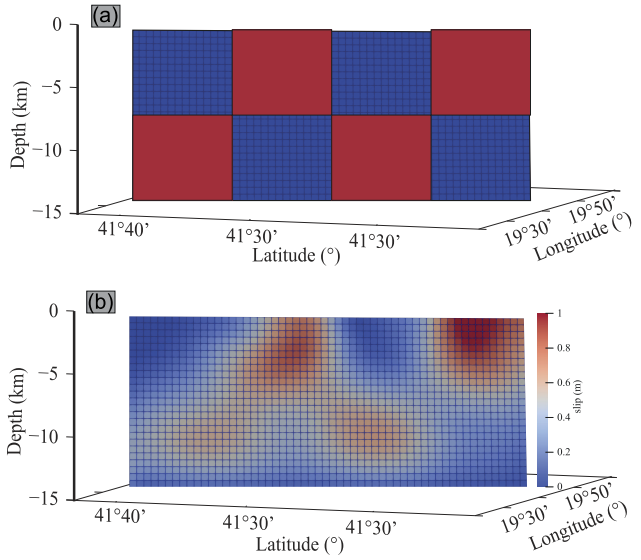

Figure C1. Resolution tests. (a) Input model located at a depth of 0–23 km with a uniform slip of 1 m; (b) modelled coseismic slip using a synthetic pair of data generated from GTdef for the GPS stations and INSAR.

APPENDIX C: CHECKERBOARD TEST

C.1 CHECKERBOARD TEST

We performed checkerboard tests to examine the resolution of our model (Fig. C1a–b, Fig. C2a–b and Fig. C3a–b). We produced synthetic displacements for both GNSS and INSAR data using the GTdef software (Chen *et al.* 2009; Murekezi *et al.* 2020). Using these synthetic displacements, we used the SDM software to identify the patches introduced in our synthetic forward models and then to compare the output slip distributions. The test considered six patches with a reverse slip of 1 m and six patches with 0 m displacement (Fig. C1a) on the fault located between 0 and 23 km in depth. To test the detection of a single patch, like our coseismic slip distribution, we performed also two tests considering a rectangular patch with a 1 m reverse slip (Figs C2a and C3a) using the geometric parameters of our best model. On the first test the patch is located in the same depth range as our best model (15–20 km depth; Fig. C2a) and the second test the patch is located deeper (20–25 km depth; Fig. C2a).

We can conclude that, in this case, the SDM software could accurately reproduce the patch (location and slip amplitude) when it is located at 15–17 km depth (Figs C1b and C2b), however, it did not precisely reproduce the patch when this one is located deeper (Figs C1b and C3b). Thus, the SDM software has then a better resolution when the source is at located between the surface and 20 km depth. Since our best model slip is located at a depth of 15–20 km depth, we can suppose that it is well located and that the slip distribution is well described.

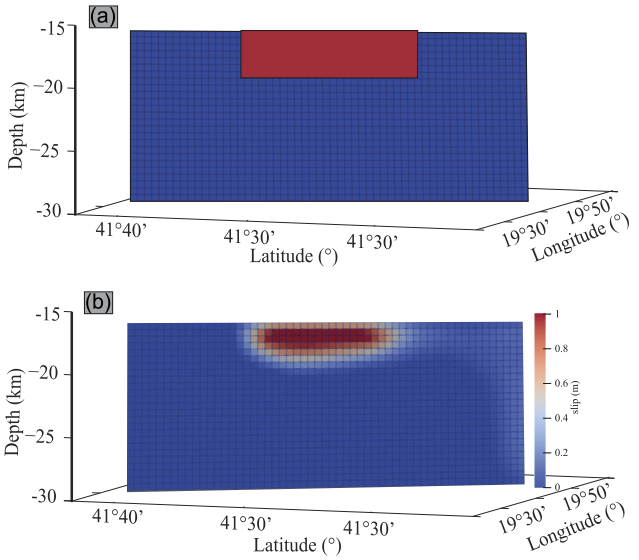

Figure C2. Resolution tests. (a) Input model located at 15–20 km at a uniform slip of 1 m. (b) Modleled coseismic slip using a synthetic pair of the data generated from GTdef for the GPS stations and INSAR.

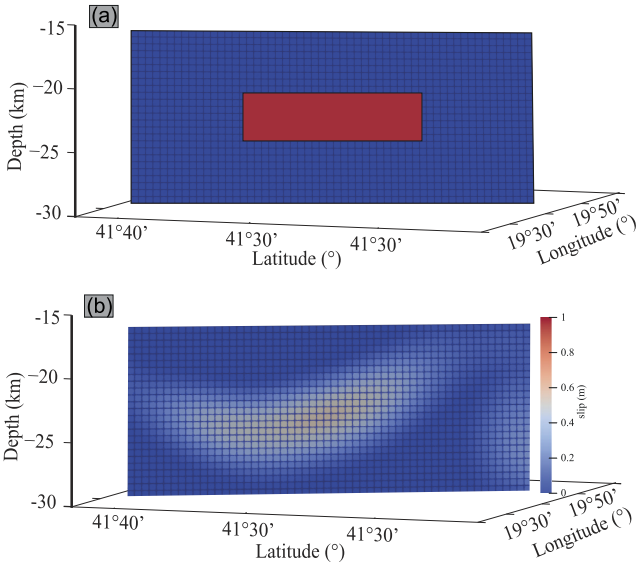

Figure C3. Resolution tests. (a) Input model located at a depth of 20–25 km on the fault with a uniform slip of 1 m; (b) modelled coseismic slip using a synthetic pair of data generated from GTdef for the GPS stations and INSAR.